MANTLE VS. CRUST: UNTANGLING INFLUENCES ON OCEAN ISLAND BASALT STABLE O AND H ISOTOPIC COMPOSITION VIA TANDEM OLIVINE-GLASS ANALYSES AT KAMA‘EHUAKANALOA VOLCANO, HAWAI‘I

A THESIS SUBMITTED TO THE GRADUATE DIVISION OF THE UNIVERSITY OF HAWAI‘I AT MĀNOA IN PARTIAL FULFILLMENT OF THE REQUIREMENTS FOR THE DEGREE OF

MASTER OF SCIENCE

IN

EARTH & PLANETARY SCIENCES

DECEMBER 2022

By

Molly Jean Cunningham

Thesis Committee:

Aaron J. Pietruszka, Chairperson

Michael O. Garcia

Kevin T. M. Johnson

Keywords: Oxygen isotopes, hydrogen isotopes, magmatic assimilation, Hawaiian volcanoes, mantle, seamount

ACKNOWLEDGEMENTS

I'd like to thank my family: Mom, Dad, and Amelia, my success is yours because it grows from your support. Thank you for your love from the other side of the ocean.

I'd like to thank my advisor, Aaron Pietruszka. I've gained immeasurable skills in scientific analysis, thoughtfulness, and patience from you. Thank you for introducing me to so many powerful educational experiences in academia. You are remarkable for your care and dedication to your field, and I am immensely grateful for your guidance throughout my degree.

I'd like to thank Mike Garcia. You have genuinely pushed me to be my best at every opportunity. Without that pressure, I would not have grown (like clinopyroxene in basaltic melts) into the scientist I am today. Thank you for believing in my potential.

I'd like to thank Kevin Johnson. You jumped onto my thesis committee in a time of urgency and you reminded me of how much I love marine geochemistry. Thank you for reigniting my passion and reassuring me of my value to the scientific community.

I'd like to thank Jasper Konter and Bridget Smith-Konter, my mentors and first believers. I would never have made it to Honolulu without the Earth Science on Volcanic Islands Research Experience for Undergraduates. In 2019, this program introduced me to volcano studies, my future advisors, and my closest friends – this program introduced me to my future. Your joy and commitment to excellence gave me the dream of being a volcanologist. It is heartbreaking to complete this journey without both of you here.

I'd like to thank Kendra Lynn for investing her time and energy in the success of young women in STEM. Thank you for revising writing drafts with me for hours, sitting with me through tears, and cheering me on when I couldn't even cheer for myself. I owe you the world, and coffee.

I'd like to thank Ilya Bindeman, Joe Boro, and Dale Burns for their assistance in data collection and analysis for this project. These datasets would not exist without their patience and expertise.

I'd like to thank William Nelson. Thank you for your compassion when I needed it most. I will always be grateful for your Scottish tea and for dropping everything to tackle the electron microprobe with me. I appreciate you.

I'd like to thank Lily Shao. Thank you for countless emails, answers, and tissues. You are the reason the entire Department of Earth Sciences remains functional, and you're the reason I'm able to graduate.

I'd like to thank my best friends on Earth: Natália Gauer Pasqualon and Devon Wolfe. Thank you for your unwavering support, in every cup of coffee, every sunset surf session, and every midnight phone call. You clear my mind and have my heart. I love you.

This list would continue forever if I could thank everyone who built me up over the past two years. This thesis is a representation of the scientist I am today, and I am that person because of you all. *Thank you.*

ABSTRACT

The stable O and H isotopic composition of ocean island basalts reflect the interplay of deep and shallow magmatic processes such as melting of a heterogeneous mantle source and crustal contamination. For Hawaiian volcanoes, it has been debated whether lavas retain their source-derived isotopic compositions, or if these signatures are overprinted by assimilation of hydrothermally altered materials. New δD and $\delta^{18}O$ analyses of glass and olivine from the youngest Hawaiian volcano, Kama‘ehuakanaloa (Kama‘ehu; formerly Lō‘ihi), clarify the extent to which magmatic contamination influences O and H isotope ratios of erupted lavas. We find that in most samples, assimilation of seawater-derived fluids is minor: this process has elevated δD, Cl/K_2O, and H_2O in some glasses, but most samples retain mantle-like δD (-60 to -90‰) until eruption. In contrast, Kama‘ehu lavas demonstrate variation in olivine $\delta^{18}O$ ($\delta^{18}O_{ol}$ = ~4.5 to 5.4‰) and glass $\delta^{18}O$ ($\delta^{18}O_{gl}$ = ~5.0 to 6.2‰) that is greater than that expected from melting of simple peridotitic mantle. We find that different regions of the volcanic edifice erupt lavas that are compositionally distinct in their $\delta^{18}O$: North Rift Zone lavas are relatively ^{18}O-enriched ($\delta^{18}O_{gl}$ = ~5.6‰); South Rift Zone lavas are relatively ^{18}O-depleted ($\delta^{18}O_{gl}$ = ~5.3‰); and lavas from the summit region have intermediate $\delta^{18}O$ values ($\delta^{18}O_{gl}$ = ~5.4‰). We resolve these observations into an isotopically consistent model of the Kama‘ehu magmatic plumbing system. Over time, differences in the temperature of circulating hydrothermal fluids may have altered basalt in the volcanic edifice to high $\delta^{18}O$ in the NRZ and low $\delta^{18}O$ in the SRZ. Magmas with initial mantle-derived $\delta^{18}O$ ($\delta^{18}O_{liq}$ = ~5.4‰) ascend into the shallow volcanic plumbing system and assimilate this hydrothermally altered rock, causing individual magmas to shift toward the $\delta^{18}O$ value of local assimilants. The degree of this contamination may be greatest in the rift zones and least in the summit due to a higher rate of magma supply to the summit reservoir system. $\delta^{18}O_{ol}$ tracks with regional differences in $\delta^{18}O_{gl}$, indicating that the assimilation process begins before or during olivine fractionation. Finally, olivine entrainment and lack of homogenization prior to eruption preserve isotopic heterogeneity on small spatial scales in erupted lavas. Variations in $\delta^{18}O$ for Hawaiian lavas thus may be controlled by processes operating within the shallow volcanic plumbing system, overprinting variation derived from melting of a heterogeneous mantle source. To determine the true, mantle-derived O isotopic signature of a volcano, systematic analyses of many samples are required.

TABLE OF CONTENTS

LIST OF TABLES

LIST OF FIGURES

1. INTRODUCTION

The O and H isotopic composition of the mantle is difficult to constrain because crustal processes may modify or obscure the source-derived isotopic signatures of ascending magma. Thus, it is important to characterize these shallow processes and their effects on magmatic stable O and H isotope ratios (expressed as δD and $\delta^{18}O$). The Hawaiian Islands present a well-studied framework in which to evaluate δD and $\delta^{18}O$ systematics in the mantle, crust, and volcanic edifice (Kyser & O'Neil, 1984; Garcia et al., 1989, 1998, 2008; Eiler et al., 1996a, b; Wang et al., 2003, 2010; Wang & Eiler, 2008; Lassiter et al., 2022). Generally, Hawaiian glasses demonstrate a limited range in δD (~-90 to -60‰; Kyser et al., 1982; Garcia et al., 1989, Loewen et al., 2019), similar to that of MORB and the global average for submarine basalts (-75 ± 24‰; Dixon et al., 2017; Craig & Lupton, 1976; Rison & Craig, 1983). The observation of high $^{3}He/^{4}He$ contents (~20 to 30 R_A; e.g., Kurz et al., 1983) and δD of ~-75‰ in glasses from Kamaʻehuakanaloa Volcano (Kamaʻehu; formerly Lōʻihi) led Loewen et al. (2019) to propose that some Hawaiian glasses represent uncontaminated δD similar to primordial mantle values.

Characterization of $\delta^{18}O$ in Hawaiian rocks has been controversial. Hawaiian lavas range more widely in glass $\delta^{18}O$ ($\delta^{18}O_{gl}$ = ~4.3 to 6.5‰; Garcia et al., 1989; Garcia et al., 1998a, 2008; Wang et al., 2003, 2010) than fresh MORB glass ($\delta^{18}O_{gl}$ = ~5.4 to 5.8‰; Eiler et al., 2000; Eiler, 2001; Harmon & Hoefs, 1995). Similarly, the range of $\delta^{18}O$ observed for olivine from Hawaiian lavas ($\delta^{18}O_{ol}$ = ~3.3 to 6.0‰; Eiler et al., 1996a, b; Gaffney et al., 2004; Garcia et al., 1998a, 2008; Wang et al., 2008, 2010; Lassiter et al., 2022) is greater than that expected for mantle peridotite (4.9 to 5.5‰; Mattey et al., 1994). Broad correlations of $\delta^{18}O_{ol}$ with Sr, Nd, and/or Os radiogenic isotope ratios may suggest that Hawaiian magmas contain some component of altered oceanic crust, either entrained from the modern Pacific lithosphere (Eiler et al., 1996; Gaffney et al., 2004) or ancient and recycled in the Hawaiian plume source (Lassiter & Hauri, 1998; Wang et al., 2010). Alternatively, the isotopic range of parental melts may be limited, requiring variation to be introduced by magmatic contamination within the shallow volcanic edifice ("self-assimilation"; Lassiter et al., 2022). At Mauna Kea, continual digestion of low-$\delta^{18}O$, hydrothermally altered wall-rock during assimilation-fractional crystallization (AFC) may cause $\delta^{18}O_{ol}$ to systematically decrease with decreasing groundmass MgO contents (Wang & Eiler, 2008; Lassiter et al., 2022). Similarly, late-stage assimilation of hydrothermally altered, ^{18}O-depleted rock may explain increased olivine-glass isotopic disequilibrium in erupted glass from

the Kīlauea Puʻuʻōʻō eruption (Garcia et al., 1998a; 2008). For Hawaiian volcanoes, many processes exert a control on magmatic $\delta^{18}O$, and it remains unclear which of these is dominant for a given volcano at a given stage of its evolution.

Kamaʻehu, the youngest volcano in the Hawaiian-Emperor Chain (Moore et al., 1982), is the focus of the present study. This seamount is in transition from the pre-shield to shield stage of Hawaiian volcanism (Garcia et al., 1993) and is experiencing an increase in magma supply as it encroaches upon the axis of the Hawaiian mantle plume (e.g., Clague et al., 1987). Kamaʻehu rises from the submarine flank of Mauna Loa, ~35 km south of the southern shoreline of the Island of Hawaiʻi. Its volcanic edifice consists of a 15-km bifurcated North Rift Zone ("NRZ"), a 22-km South Rift Zone ("SRZ"), and a 2 km-wide summit caldera (Fig. 1; Clague et al., 2019; Fornari et al., 1988), with notable hydrothermal vent systems observed in both the summit region and along the SRZ (Malahoff et al., 1982; Karl et al., 1988; The Lōʻihi Science Team, 1997). Kamaʻehu is well-suited for exploring the mantle versus crust controversy of stable O and H isotopic composition because its magmas are known to experience shallow assimilation (Kent et al., 1999a, b; Dixon & Clague, 2001; Pietruszka et al., 2011), yet its glasses seem to preserve their source-derived δD values (Garcia et al., 1989; Loewen et al., 2019). Additionally, previous interpretations of Kamaʻehu lava compositions disagree on O isotopic properties of the mantle source: glass $\delta^{18}O$ values collected using conventional methods were attributed to a mantle source that is ^{18}O-depleted relative to MORB ($\delta^{18}O_{gl}$ = 4.6 to 5.1‰; Garcia et al., 1989), whereas laser-fluorination analyses yielded MORB-like olivine O compositions ($\delta^{18}O_{ol}$ = 5.2‰; Eiler et al., 1996a) and were attributed to a source with $\delta^{18}O$ similar to MORB. This study thus presents the valuable opportunity to evaluate O isotopic compositions of the Kamaʻehu source and compare the contributions of source-related vs. crustal processes on lava $\delta^{18}O$ with high-precision laser fluorination methods. This goal is accomplished via tandem olivine-glass measurements: analyses of glass characterize melt isotopic composition as erupted; analyses of olivine serve as a proxy of melt isotopic composition throughout differentiation in the volcanic plumbing system. The δD, $\delta^{18}O_{gl}$, and $\delta^{18}O_{ol}$ values presented here are interpreted in the context of glass and olivine core major element data to construct an isotopically consistent model of the Kamaʻehu shallow plumbing system and mantle source.

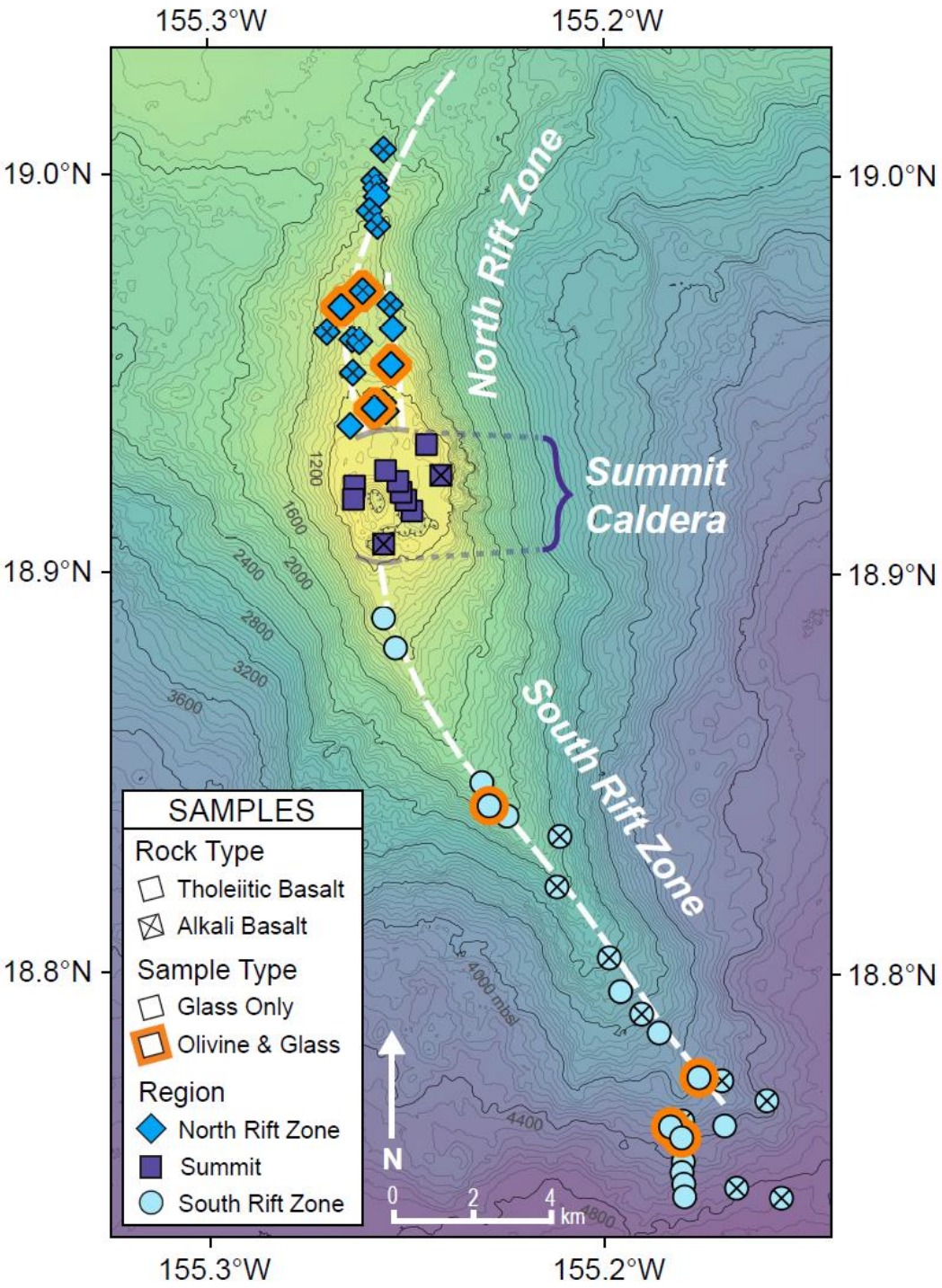

Figure 1. Bathymetric map of the Kama‘ehu volcanic edifice and sampling sites for glass and olivine. Symbols represent sites at which lava samples were collected by ROV submersible. Symbols with orange borders indicate samples selected for complementary olivine analyses. NRZ samples (medium blue diamonds) were collected by *Pisces V* in 1990 in the depth range 1150 to 1915 mbsl; summit samples (navy blue squares) were collected by *Alvin* in 1987 and *Pisces V* in 1996 in the depth range 977 to 1305 mbsl; SRZ samples (pale blue circles) were collected by *Alvin* in 1987, *Mir* in 1990, and *Shinkai 6500* in 1999 in the depth range 1320 to 5025 mbsl.

2. SAMPLING AND ANALYTICAL METHODS

This study utilized 54 tholeiitic to alkalic basalt lavas distributed across the Kamaʻehu submarine volcanic edifice (Fig. 1). All of the samples were analyzed for major, minor, and volatile (H_2O, Cl, and S) element abundances, and $\delta^{18}O$ and δD values on individual fragments of glass. Additionally, individual olivine crystals from a subset of eight samples (four each from the NRZ and SRZ) were analyzed for major and minor element abundances and $\delta^{18}O$. Major and trace element measurements were conducted on a population ($n \geq 100$) of olivine phenocryst cores for each sample. Olivine phenocrysts and crystal-free glass fragments were handpicked under a binocular microscope to avoid pieces showing any signs of post-eruptive alteration. Selected olivine phenocrysts contained <1 vol. % spinel and/or melt inclusions.

Major (Si, Ti, Al, Fe, Mg, Ca, and Na) and minor (K, Mn, and P) element abundances of Kamaʻehu glasses were measured on the five-spectrometer Cameca SX-50 electron microprobe at the University of Hawaiʻi (UH) at Mānoa (M. Garcia, analyst). Major and minor element abundances for all of the summit and a subset of the SRZ samples (1804-1. 1804-10, 490-1, 490-2, and 494-6) using this instrument are from Pietruszka et al. (2011). Reported values are the average of 5-10 spot analyses using a 15-20 μm beam diameter, 15 kV accelerating voltage, 10 nA beam current, and 40-50 s on-peak counting time for major elements, and 80-90 s on-peak counting time for minor elements. Chlorine, S, and H_2O concentrations of glasses from the summit region and the five SRZ samples (listed above) are from Pietruszka et al. (2011). All NRZ glasses were analyzed for Cl and S at Stanford University on the JEOL JXA-8230 electron microprobe (D. Burns, analyst) following the methods of Davis et al. (2003). The remaining SRZ glasses were analyzed for Cl and S at UH on the Cameca SX-50 electron microprobe (M. Garcia, analyst) using a 15 μm beam diameter, 15 kV accelerating voltage, 20 nA beam current, and 60 s on-peak counting time. The reported values are the average of 5-15 spot analyses. The relative analytical precision is 1-2% for major elements, 5-10% for minor elements, 2% for S, and 8% for Cl based on repeated analyses of the A-99 (major, minor elements only) and VG2 volcanic glass standards (Jarosewich et al., 1979).

Olivine compositions are single-spot analyses of phenocryst cores and rims identified in thin section and backscatter electron (BSE) imagery. Measurements were conducted on the five-spectrometer JEOL Hyperprobe JXA-8500F at UH using a 10 μm beam, 20 kV accelerating

voltage, 100 nA beam current, and on-peak counting time of 60 s (M. Cunningham and J. Boro, analysts). Mean-atomic-number (MAN) calculations were used to obtain background counts (Donovan & Tingle, 1996). The relative analytical precision is <1% for major elements (Si, Fe, and Mg) and 1-4% for minor elements (Ni and Ca) based on repeated analyses of San Carlos olivine (Jarosewich et al., 1980).

The $\delta^{18}O$ values of glass fragments and olivine phenocrysts were determined using the laser fluorination method and a gas source MAT 253 isotope ratio mass spectrometer (IRMS; Bindeman et al., 2012, 2020). Adhering glass was removed from olivine crystals prior to analysis using 1-2 treatments with fluoroboric acid (HBF_4) and two rinses with distilled water in an ultrasonic bath after neutralization of the acidic solution with sodium carbonate (Na_2CO_3). The δD values and the total H_2O abundances of the glasses were measured with a high-temperature conversion elemental analyzer (TC/EA) interfaced with the IRMS, using the methods described in Martin et al. (2017) and Loewen et al. (2019). All O and H isotope compositions are expressed relative to Vienna Standard Mean Ocean Water (VSMOW).

The precision of $\delta^{18}O$ for glass and olivine in this study are estimated based on repeated analyses of in-house reference materials. Relative analytical precision of glass is based on a total of 34 $\delta^{18}O$ analyses of Menehune, a volcanic glass quenched from the Pu‘u‘ō‘ō eruption of Kīlauea Volcano (Hawai‘i). Menehune glass reproduced to ± 0.15‰ (±2SD). Relative analytical precision of olivine is based on a total of five $\delta^{18}O$ analyses of San Carlos olivine (Jarosewich et al., 1980; Bindeman et al., 2006), which reproduced to ± 0.24‰ (±2SD). Relative analytical precision of δD and H_2O measurements are 1-3‰ and 0.05 wt. % as reported in Bindeman et al. (2020). All uncertainties in this study are given ±2SD unless otherwise noted.

3. RESULTS

3.1. GLASS MAJOR & VOLATILE ELEMENT COMPOSITION

Kama‘ehu glasses have compositions ranging from tholeiitic basalt to hawaiite (Table 1; Fig. 2). Samples are categorized as tholeiitic or alkalic according to their alkalic index (see Table 1 caption; A.I.: < 0 tholeiitic, > 0 alkalic; Macdonald & Katsura, 1964; e.g., Yang et al., 1996), although some could be considered transitional. Tholeiitic and alkalic basalt lavas are found in all regions of the volcanic edifice (Fig. 1). The NRZ demonstrates the greatest compositional diversity with the highest proportion of alkalic samples (70%), including three hawaiite glasses. In contrast, SRZ samples are mostly tholeiitic basalts (62%). Of the nine alkalic SRZ glasses, three plot within error (<0.1 wt.%) of the trendline between alkalic and tholeiitic basalts (Macdonald & Katsura, 1964). The summit samples include eight tholeiitic basalts and two mildly alkalic basalts.

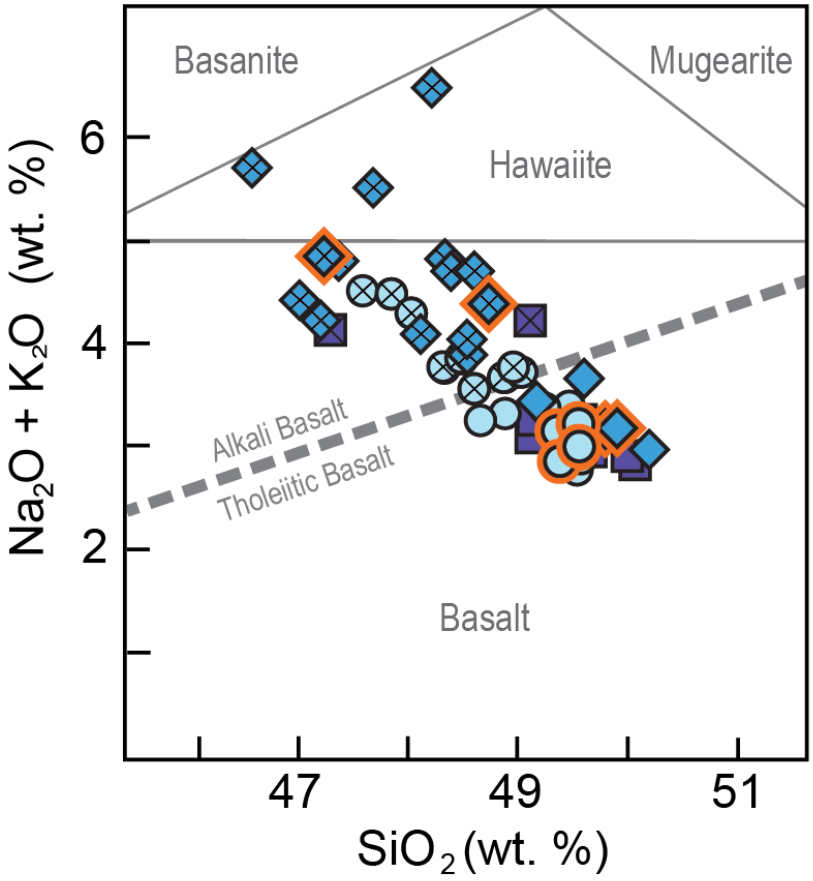

Figure 2. Total alkali-silica diagram of Kama‘ehu glasses.
Using the classification scheme of sodic and potassic basalts described by Le Maitre et al. (2002). Trendline between tholeiitic and alkali basalt given by Macdonald & Katsura (1964). Symbol descriptions given in Fig. 1. Analytical error is smaller than symbol size.

Table 1. Major and minor element concentrations from EPMA and total H_2O concentrations from E/A-IRMS of Kama'ehu glasses. Values given in wt. % unless otherwise indicated. Totals include volatile element (H_2O, Cl, S) abundances. Values are normalized to totals of 100% prior to plotting in figures.
[a] A.I.: Alkalic index = $(Na_2O+K_2O)-[(0.37*SiO_2)-14.43]$; from Macdonald & Katsura (1964), based on trendline separating tholeiitic and alkalic basalts
[b] Samples with major, minor, Cl, and S concentrations reported in Pietruszka et al. (2011)

Sample	Region	Depth (m)	A.I.[a]	SiO_2	TiO_2	Al_2O_3	FeO^T	MgO	CaO	Na_2O	K_2O	P_2O_5	MnO	H_2O	Cl (ppm)	S (ppm)	Totals
145-1	NRZ	1915	0.7	47.48	3.45	14.36	12.4	5.60	10.88	3.17	0.86	0.38	0.19	0.75	286	1640	99.52
145-8	NRZ	1805	1.3	47.8	3.56	14.65	12.67	4.90	9.97	3.56	1.11	0.48	0.20	0.96	464	1179	99.86
146-1	NRZ	1770	2.3	47.01	4.13	14.45	12.87	4.56	9.60	4.17	1.26	0.43	0.19	0.94	535	1173	99.61
146-3a	NRZ	1690	-0.3	48.62	3.02	13.95	12.42	6.10	11.01	2.79	0.61	0.27	0.20	0.65	533	1361	99.64
146-4	NRZ	1640	3.1	47.22	3.65	15.09	11.65	4.28	9.09	4.77	1.57	0.52	0.18	1.07	821	1795	99.09
146-5	NRZ	1595	1.2	46.48	3.46	14.33	12.95	5.57	11.02	3.3	0.87	0.36	0.21	0.84	766	1900	99.39
147-2	NRZ	1490	1.8	46.8	3.32	14.75	12.69	5.35	10.86	3.67	1.12	0.39	0.20	0.73	734	1809	99.88
147-3	NRZ	1425	0.8	48.8	3.42	14.50	12.07	5.60	10.92	3.28	1.10	0.35	0.19	0.82	-	-	101.05
147-4	NRZ	1420	1.2	48.57	3.43	14.37	11.89	5.66	10.88	3.67	1.03	0.37	0.19	0.69	926	1949	100.75
155-2	NRZ	1315	0.4	48.37	3.33	14.22	11.67	6.21	11.57	3.08	0.79	0.35	0.18	0.79	1042	1171	100.56
155-4	NRZ	1260	0.5	48.38	3.18	14.31	12.41	5.75	11.16	3.20	0.82	0.35	0.22	0.61	752	1938	100.39
156-1	NRZ	1170	-1.2	49.79	2.75	14.00	11.13	6.58	11.72	2.51	0.43	0.23	0.17	0.52	724	1898	99.83
156-6	NRZ	1150	-0.9	49.40	2.77	13.11	11.4	6.99	11.95	2.33	0.76	0.24	0.15	0.57	994	1898	99.67
156-8	NRZ	1220	1.7	46.77	3.52	15.02	12.39	5.06	10.78	3.54	1.20	0.44	0.15	0.8	965	1703	99.67
157-1	NRZ	1485	-0.3	49.20	3.26	14.06	11.88	5.98	10.82	2.91	0.71	0.3	0.17	0.75	951	1704	100.04
157-2	NRZ	1535	1.4	47.53	3.46	14.76	12.3	4.95	10.12	3.64	1.09	0.39	0.18	0.92	800	1746	99.34
157-5	NRZ	1440	2.9	46.24	3.88	14.93	12.47	4.92	10.55	4.20	1.45	0.53	0.17	0.92	945	1523	100.26
157-6	NRZ	1450	1.5	46.44	3.46	12.51	12.34	6.88	12.24	3.33	1.03	0.43	0.17	0.88	1002	1721	99.71
157-7	NRZ	1325	-0.8	49.32	2.79	13.31	11.69	6.67	11.68	2.36	0.77	0.24	0.19	0.70	1094	1806	99.72
157-8	NRZ	1160	-0.9	49.56	2.88	13.31	11.78	6.59	11.74	2.4	0.75	0.25	0.15	0.67	1295	1788	100.08
1804-1[b]	SRZ	1357	-1.0	49.19	2.46	13.35	11.40	7.29	12.21	2.40	0.49	0.21	0.19	0.45	447	1698	99.64
1804-10[b]	SRZ	1320	-1.1	49.20	2.56	12.93	11.46	8.01	12.02	2.35	0.44	0.21	0.16	0.40	443	911	99.74
2335-5	SRZ	5025	0.0	47.84	2.98	13.97	10.82	6.82	11.95	2.81	0.71	0.33	0.15	0.71	932	1526	99.10
2338-1a	SRZ	4930	0.4	47.73	3.05	14.20	11.38	6.18	11.58	3.01	0.79	0.35	0.15	0.75	313	1702	99.17
2343-13	SRZ	3179	1.0	47.44	3.23	14.26	11.37	6.12	11.47	3.37	0.91	0.38	0.17	1.07	1096	1624	99.79
2343-6	SRZ	3598	1.3	47.07	3.36	14.85	11.70	5.73	11.09	3.45	1.03	0.44	0.16	0.77	400	1858	99.64

Table 1. (Continued) Major and minor element concentrations from EPMA and total H_2O concentrations from E/A-IRMS of Kama‘ehu glasses.

Sample	Region	Depth (m)	A.I.[a]	SiO_2	TiO_2	Al_2O_3	FeO^T	MgO	CaO	Na_2O	K_2O	P_2O_5	MnO	H_2O	Cl (ppm)	S (ppm)	Totals
2343-9	SRZ	3479	-0.3	48.59	2.94	13.54	11.69	6.87	11.92	2.66	0.66	0.32	0.17	0.71	1093	1727	100.06
490-1	SRZ	4684	0.3	47.62	2.96	14.07	11.49	6.56	11.76	2.97	0.76	0.31	-	0.71	1093	1727	99.20
490-2	SRZ	4657	-0.4	47.96	2.92	13.93	11.19	6.31	11.50	2.77	0.53	0.25	-	1.67	360	2035	99.02
490-3	SRZ	4657	-0.7	48.45	2.91	14.26	11.24	6.47	11.48	3.03	0.64	0.30	-	1.45	1125	1764	100.24
490-5	SRZ	4598	-0.7	47.96	2.83	13.52	10.92	6.63	11.75	2.53	0.50	0.27	0.16	1.37	424	1730	98.44
490-6	SRZ	4494	-1.0	48.02	2.91	13.77	11.28	6.11	11.24	2.62	0.52	0.26	0.18	1.45	419	1786	98.35
490-7	SRZ	4426	-0.8	47.89	2.71	12.82	10.95	7.23	12.20	2.33	0.43	0.22	0.16	1.42	958	2079	98.36
490-8	SRZ	4401	-0.5	47.88	2.80	13.42	11.01	6.65	11.70	2.50	0.50	0.28	0.16	0.76	1267	1568	97.66
491-2	SRZ	4300	0.0	48.42	3.03	13.96	11.34	6.06	11.24	2.75	0.58	0.31	0.15	0.69	584	1904	98.54
491-5	SRZ	4383	0.1	48.87	2.98	14.30	11.17	6.72	11.42	3.09	0.66	0.34	0.17	0.73	-	-	100.45
494-5	SRZ	2358	-0.8	48.81	2.87	14.02	12.07	6.20	11.25	2.59	0.47	0.28	0.19	0.61	531	1861	99.36
494-6	SRZ	2323	-0.9	49.06	2.68	13.99	12.05	6.40	11.56	2.53	0.44	0.25	-	0.59	765	1571	99.56
494-8	SRZ	2171	-0.7	48.96	2.99	13.87	12.20	6.02	11.07	2.66	0.52	0.30	0.19	0.60	443	1608	99.37
512-1	SRZ	2643	0.0	47.77	3.44	14.39	12.09	5.50	10.75	3.42	0.95	0.45	0.17	0.60	627	1731	99.53
513-2	SRZ	4340	-0.3	48.06	2.98	13.16	11.50	7.19	12.13	2.57	0.66	0.30	0.17	0.72	799	1850	99.43
513-7A	SRZ	3936	-0.6	49.46	2.77	13.80	11.31	7.00	11.85	2.77	0.53	0.28	0.18	0.68	950	1850	100.63
513-7B	SRZ	3936	-0.7	49.51	2.72	13.60	11.28	7.32	11.86	2.72	0.53	0.26	0.17	0.67	730	2147	100.65
515-1	SRZ	3060	1.2	46.60	3.29	14.57	11.46	5.47	11.04	3.41	0.97	0.40	0.17	1.04	699	2183	98.42
1801-1[b]	Summit	1305	-1.0	48.75	2.63	13.70	11.80	6.91	12.05	2.53	0.45	0.24	0.14	0.68	687	1909	99.88
1801-11[b]	Summit	1248	-1.3	48.77	2.64	13.63	11.73	6.82	11.90	2.36	0.44	0.21	0.20	0.49	239	1585	99.19
1801-16[b]	Summit	1110	-0.7	49.49	2.44	13.55	11.94	6.93	11.45	2.40	0.38	0.21	0.18	0.52	246	1333	99.49
1801-19[b]	Summit	1062	-0.6	49.13	2.82	13.86	11.67	6.49	11.53	2.56	0.60	0.25	0.16	0.55	293	1813	99.62
1801-22[b]	Summit	987	-1.1	48.67	2.87	13.75	11.74	6.71	11.69	2.58	0.57	0.24	0.21	0.46	194	1452	99.49
1802-22[b]	Summit	998	-1.0	49.31	2.61	13.84	11.84	6.80	11.65	2.41	0.42	0.20	0.18	0.53	199	1445	99.79
1803-14[b]	Summit	1140	1.1	49.20	2.61	13.71	12.00	6.80	11.72	2.48	0.42	0.27	0.18	0.74	249	1553	100.13
1803-16[b]	Summit	977	-1.4	47.12	3.88	14.17	13.10	5.49	11.10	3.31	0.84	0.38	0.18	0.39	371	1474	99.96
1804-19[b]	Summit	1020	0.50	49.69	2.48	13.26	11.52	7.50	11.72	2.33	0.36	0.18	0.18	0.80	353	1381	100.02
P286-1F[b]	Summit	1050	-0.8	48.73	3.76	13.82	12.75	5.17	10.21	3.33	0.89	0.34	0.19	0.53	932	872	99.72

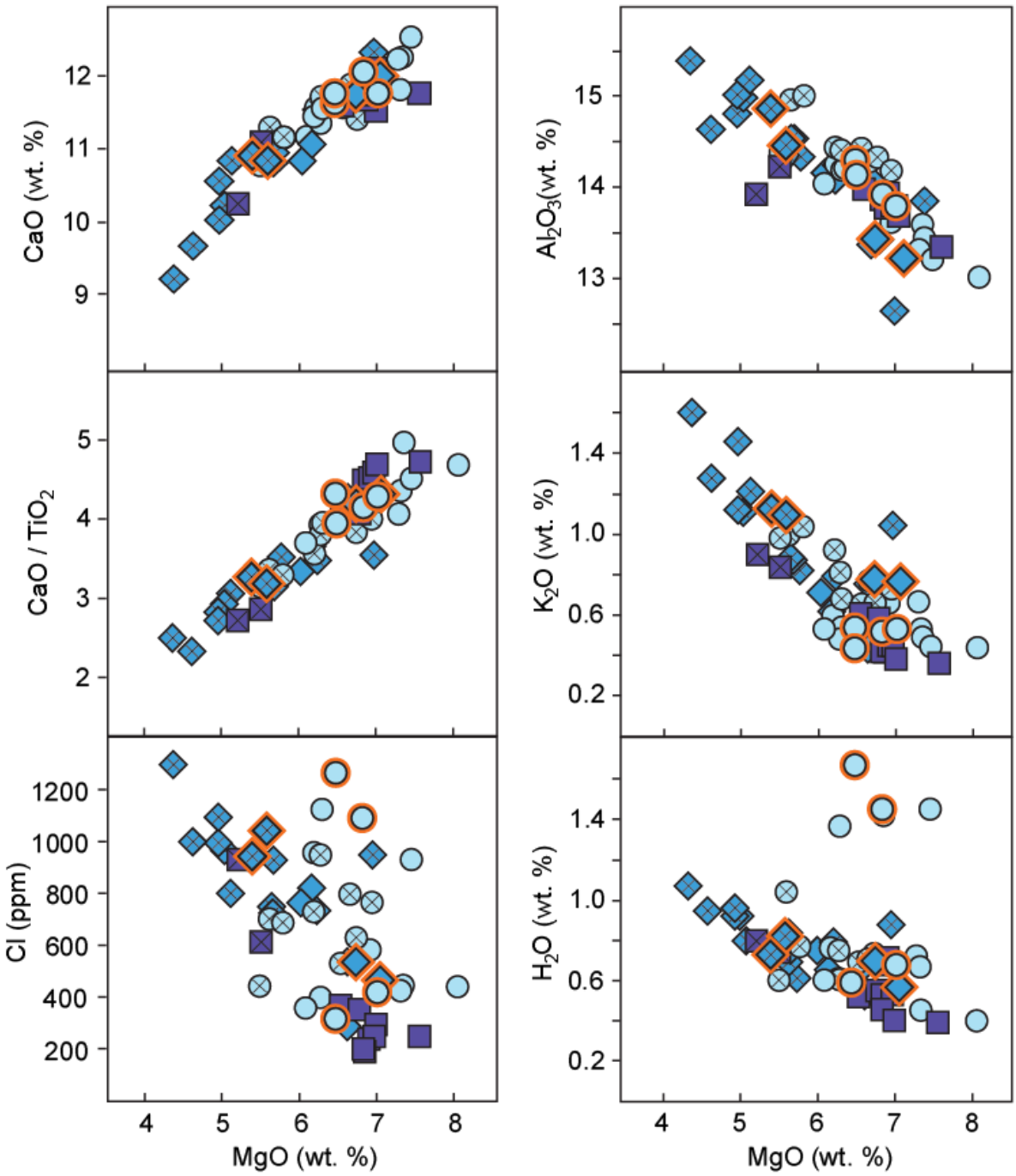

Figure 3. MgO variation diagrams for CaO, Al_2O_3, CaO/TiO_2, K_2O, Cl, and H_2O concentrations of Kama'ehu glasses. Note the similarity in trends of K_2O, Cl, and H_2O: these increase in abundance with decreasing MgO, indicating incompatible behavior during fractional crystallization. Some samples have decoupled Cl and H_2O at moderate MgO contents (~6 to 7 wt. %). Symbol descriptions are given in Fig. 1. Error bars are smaller than symbol size.

MgO contents range from 4.3 to 8.0 wt. % (Fig. 3). NRZ glasses present the lowest MgO values (4.3 to 7.0 wt. %), SRZ glasses have the highest MgO values (5.5 to 8.0 wt. %), and summit glasses have intermediate values (5.2 to 7.5 wt. %). Together, these glasses form relatively coherent trends on MgO variation diagrams (Fig. 3). The low-MgO glasses tend to be alkalic basalts and the higher-MgO glasses tend to be tholeiitic basalts, although there is considerable overlap between rock types. Across the NRZ, SRZ, and summit region, K_2O and Al_2O_3 abundances increase and CaO abundances decrease with decreasing MgO contents. The pattern of decreasing CaO/TiO_2 with decreasing MgO is consistent with the dominant fractionation of clinopyroxene from Kama‘ehu melts at relatively high MgO contents (~8 wt.%). This contrasts with Kīlauea, where clinopyroxene starts to crystallize at a range in MgO contents between 7.0 and 7.5 wt. % MgO, depending on the melt composition (e.g., Wright & Fiske, 1971; Garcia et al., 2003).

Glass total H_2O contents vary from ~0.4 to 1.7 wt. % and Cl concentrations vary from ~200 to 1300 ppm (Table 1). Both Cl and H_2O abundances increase with decreasing MgO, and both can be highly variable at a given MgO content (Fig. 3). Between 6 and 7 wt. % MgO, for example, Cl and H_2O abundances vary over almost the entire range observed in this study. This scatter is most evident in glasses from the SRZ, but persists in the NRZ and, to a lesser extent, the summit region. Sulfur abundances vary from ~870 to ~2200 ppm and demonstrate no systematic relationship with MgO content (Table 1). Neither Cl, S, nor H_2O vary systematically with glass alkali content (Table 1). Sulfur abundances are not discussed further because behavior of magmatic S is nontrivially related to temperature, oxygen fugacity, and degassing history (e.g., Wallace & Carmichael, 1992), which are topics beyond the scope of this study.

3.2.OLIVINE MAJOR & MINOR ELEMENT COMPOSITION

Olivine core compositions for eight samples (Table 2; Fig. 4) range from “primitive” ($>Fo_{88}$) to “evolved” ($<Fo_{81}$) with a total range of Fo_{91} to Fo_{77}. Most of the eight samples (n = 5) show a narrow distribution in olivine composition at moderate Fo contents (e.g., Fo_{86} to Fo_{82}) and extrema reaching to both high- and low-Fo contents. The remaining three samples exhibit wide, right-skewed distributions of olivine composition with maxima at moderate to primitive forsterite contents (e.g., Fo_{86} to Fo_{88}) and tails extending toward more evolved compositions. Lavas of each distribution type are observed along both the NRZ and SRZ.

Table 2. Forsterite contents and major and minor element concentrations of olivine cores in individual Kama'ehu lavas from EPMA. Data presented are the averages of analyses from a representative population ($n \geq 100$) of olivine cores for each lava sample. Cores were identified from sample thin sections via backscatter electron (BSE) imagery. Fo = forsterite content; [Mg/(Mg + Fe)]*100.

Sample	Region	n	Fo		Major Elements (Avg)			Trace Elements (Avg)	
			Avg ± SD (2σ)	Range	SiO_2	MgO	FeO	CaO	NiO
147-2	NRZ	100	85.7 ± 2.2	83.4 - 90.6	39.71	45.30	13.51	0.33	0.31
147-3	NRZ	112	87.0 ± 3.5	77.9 - 90.7	39.88	46.33	12.37	0.30	0.33
156-6	NRZ	170	83.0 ± 2.2	81.0 - 89.3	39.31	43.52	15.89	0.30	0.23
157-7	NRZ	102	83.4 ± 3.6	82.2 - 89.6	39.46	43.82	15.53	0.30	0.23
490-2	SRZ	183	85.5 ± 3.4	77.0 - 89.0	39.76	45.71	13.77	0.29	0.31
490-3	SRZ	168	85.7 ± 3.0	79.5 - 88.7	39.92	45.91	13.61	0.28	0.32
494-6	SRZ	178	81.8 ± 2.0	80.1 - 87.8	39.34	43.19	17.14	0.31	0.21
513-7A	SRZ	172	84.7 ± 1.5	81.9 - 86.8	39.85	45.17	14.57	0.30	0.29

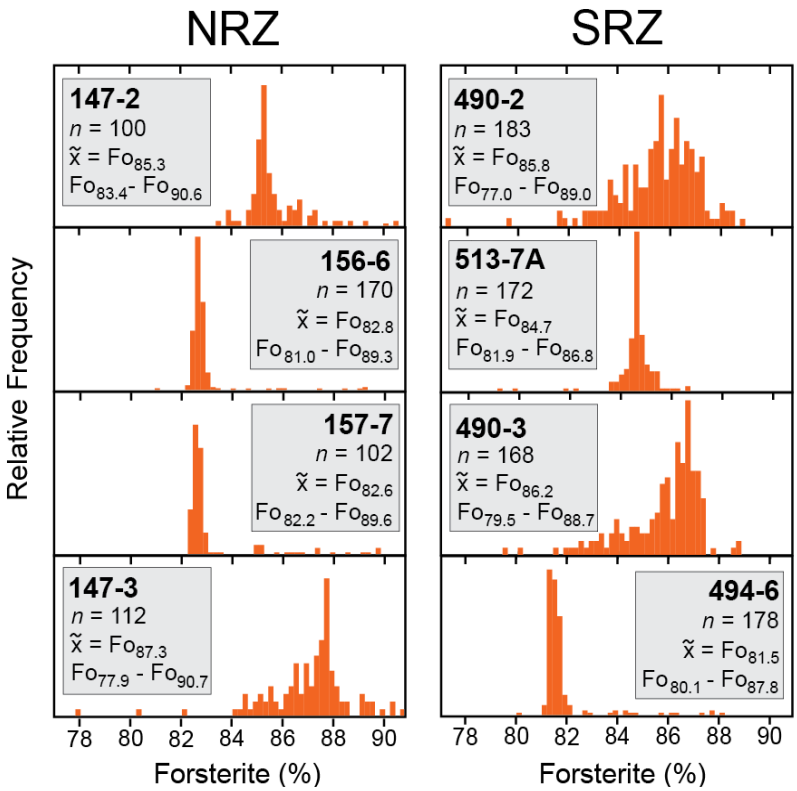

Figure 4. Distributions of forsterite contents of olivine cores within single samples. 147-2, 156-6, 157-7, 513-7A, and 494-6 demonstrate narrow distributions with low-frequency tails (i.e., few crystals have compositions corresponding to the tails of the distribution). 147-3, 490-2, and 490-3 demonstrate wide, right-skewed distributions with moderate-frequency tails (i.e., several crystals have compositions corresponding to the tails of the distribution). Both distribution types may have tails extending to primitive (>Fo_{88}) and evolved (<Fo_{81}) compositions. Lavas of each distribution type occur along both the SRZ and NRZ.
Distribution maxima are represented by the sample median, x̃. Analytical error is approximately equal to width of histogram bars (0.2%).

3.3. GLASS & OLIVINE STABLE O ISOTOPIC COMPOSITION

Single $\delta^{18}O$ analyses ("single analyses") of glass range by 1.2‰ (5.0 to 6.2‰) and have an average of 5.4 ± 0.4‰, which overlaps with the range of fresh MORB glass (Eiler et al., 2000). Single olivine analyses range by 0.9‰ (4.5 to 5.4‰) and have an average of 5.0 ± 0.4‰, which overlaps with the range of olivine in mantle peridotite (4.9 to 5.5‰; Mattey et al., 1994) (Table 3; Fig. 5). When analyses are averaged first on a sample-by-sample basis ("sample-averaged analyses"), the total range of glass $\delta^{18}O$ is 5.1 to 5.7‰, with an average of 5.4 ± 0.3‰; the total range of olivine $\delta^{18}O$ is 4.9 to 5.2‰, with an average of 5.0 ± 0.2‰ (±2SD). Thus, the sample-averaged dataset for both glass and olivine has a reduced range of $\delta^{18}O$ but an average that is indistinguishable from the average of the dataset of single analyses [two-tailed *t*-test for Independence of Samples (α = 0.05) returns p = 0.99 for comparison of olivine single analyses vs. sample-averaged analyses; p = 0.76 for comparison of glass single analyses vs. sample-averaged analyses]. For both glass and olivine, NRZ samples are offset to relatively high $\delta^{18}O$ values, whereas SRZ samples are offset to relatively low $\delta^{18}O$ values. The summit samples have intermediate glass $\delta^{18}O$ values. These regional geographic differences are statistically significant for both glass and olivine (Table 4).

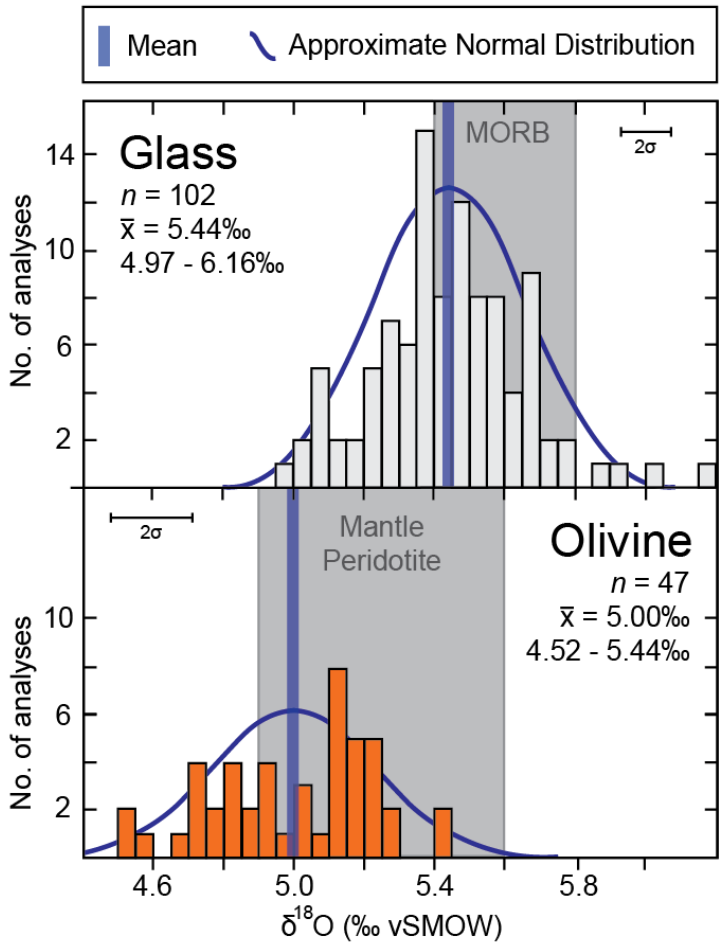

Figure 5. Distributions of single glass and olivine $\delta^{18}O$ analyses. Vertical blue lines represent sample means ($\bar{x}$). Curved solid blue lines represent approximate normal distributions with the mean and standard deviation of the glass or olivine dataset. MORB glass compositions taken from Eiler et al. (2000). Mantle peridotite olivine compositions taken from Mattey et al. (1994). The glass dataset consists of 102 single analyses from 54 lava samples. The olivine dataset consists of 47 single analyses from 8 lava samples. Histogram bars are 0.05‰ wide.

Table 3. Olivine and glass stable O and H isotope ratios, with glass H_2O and Cl concentrations. Stable isotope ratios are reported in delta (δ) notation relative to Vienna Standard Mean Ocean Water (VSMOW): $\delta D = [(D/H_{sample} - D/H_{standard})/ D/H_{standard}]*1000$; $\delta^{18}O = [(^{18}O/^{16}O_{sample} - {}^{18}O/^{16}O_{standard})/ {}^{18}O/^{16}O_{standard}] *1000$. For both glass and olivine, the observed variation in individual analyses should be considered a minimum because some analyses represent the average of two glass pieces.

Sample	Region	H_2O (wt. %)	Cl (ppm)	δD (‰)	Glass $\delta^{18}O$ (‰)			Olivine $\delta^{18}O$ (‰)		
					Mean	Range	n	Mean	Range	n
145-1	NRZ	0.75	926	-72.3	5.38					
145-8	NRZ	0.96	994	-65.9	5.46					
146-1	NRZ	0.94	1002	-71.4	5.57					
146-3b	NRZ	0.65	821	-74.9	5.78					
146-4	NRZ	1.07	1295	-72.7	5.55 ± 0.15	5.47 - 5.65	3			
146-5	NRZ	0.84	724	-65.9	5.55 ± 0.23	5.43 - 5.70	2			
147-2	NRZ	0.73	945	-76.7	5.57 ± 0.13	5.49 - 5.66	4	4.91 ± 0.28	4.74 - 5.15	5
147-3	NRZ	0.82	1042	-70.5	5.71 ± 0.42	5.5 - 6.01	5	5.02 ± 0.37	4.71 - 5.26	7
147-4	NRZ	0.69	752	-75	5.6					
155-2	NRZ	0.79	734	-71.7	5.56					
155-4	NRZ	0.61	-	-75.2	5.8					
156-1	NRZ	0.52	286	-72.7	5.37					
156-6	NRZ	0.57	464	-79.4	5.65 ± 0.39	5.36 - 5.91	4	5.15 ± 0.32	4.85 - 5.42	7
156-8	NRZ	0.80	800	-70.4	5.69 ± 0.67	5.39 - 6.16	3			
157-1	NRZ	0.75	766	-73.8	5.5					
157-2	NRZ	0.92	965	-68.9	5.4					
157-5	NRZ	0.92	1094	-70.7	5.57					
157-6	NRZ	0.88	951	-74.8	5.38					
157-7	NRZ	0.70	533	-81	5.54 ± 0.39	5.26 - 5.68	4	5.18 ± 0.17	5.05 - 5.27	5
157-8	NRZ	0.67	535	-80.4	5.68					
1804-1	SRZ	0.45	447	-75.4	5.44	5.43 - 5.45	2			
1804-10	SRZ	0.40	443	-82.9	5.5	5.47 - 5.52	2			
2335-5	SRZ	0.71	765	-68.8	5.39					
2338-1a	SRZ	0.75	950	-64.6	5.62					
2343-13	SRZ	1.07	730	-65.7	5.39					
2343-6	SRZ	0.77	687	-82.9	5.49					
2343-9	SRZ	0.71	584	-74.5	5.35					
490-1	SRZ	0.71	799	-61.2	5.53	5.52 - 5.55	2			
490-2b	SRZ	1.67	1267	-28.7	5.1 ± 0.21	4.97 - 5.23	4	4.89 ± 0.44	4.52 - 5.20	7
490-3b	SRZ	1.45	1093	-28.9	5.16 ± 0.19	5.01 - 5.31	8	5.02 ± 0.50	4.71 - 5.44	5
490-5b	SRZ	1.37	1125	-32.5	5.16					
490-6b	SRZ	1.45	932	-27.1	5.09					
490-7b	SRZ	1.42	1096	-31.2	5.09					
490-8	SRZ	0.76	958	-61.4	5.27					
491-2	SRZ	0.69	531	-65.5	5.3	5.21 - 5.38	2			
491-5	SRZ	0.73	627	-67.2	5.36					
494-5	SRZ	0.61	400	-69	5.34					
494-6	SRZ	0.59	313	-64.7	5.24 ± 0.32	5.11 - 5.32	4	4.91 ± 0.44	4.56 - 5.19	6
494-8	SRZ	0.60	360	-78.1	5.27					
512-1	SRZ	0.60	443	-78	5.57					
513-2	SRZ	0.72	-	-63.9	5.36					
513-7B	SRZ	0.68	419	-71.8	5.39 ± 0.44	5.06 - 5.59	4	4.93 ± 0.50	4.54 - 5.22	5
513-7B	SRZ	0.67	424	-71.6	5.45					
515-1	SRZ	1.04	699	-67.1	5.44					
1801-1	Summit	0.68	239	-79.2	5.34	5.27 - 5.40	2			

Table 3. (Continued) Olivine glass stable O and H isotope ratios, with glass H_2O and Cl concentrations.

Sample	Region	H_2O (wt. %)	Cl (ppm)	δD (‰)	Glass $\delta^{18}O$ (‰)			Olivine $\delta^{18}O$ (‰)		
					Mean	Range	n	Mean	Range	n
1801-11	Summit	0.40	293	-73.8	5.39	5.36 - 5.43	2			
1801-16	Summit	0.52	371	-71.6	5.46	5.43 - 5.50	2			
1801-19	Summit	0.55	353	-80.7	5.5	5.48 - 5.53	2			
1801-22	Summit	0.46	194	-76.4	5.45	5.42 - 5.47	2			
1802-22	Summit	0.53	199	-73.5	5.34	5.30 - 5.39	2			
1803-14	Summit	0.74	613	-79.5	5.39	5.34 - 5.43	2			
1803-16	Summit	0.39	246	-75.1	5.63	5.62 - 5.65	2			
1804-19	Summit	0.80	932	-78.9	5.67	5.65 - 5.69	2			
P286-1F	Summit	0.53	249	-72.8	5.34	5.22 - 5.45	2			

Notably, Kama‘ehu lavas also demonstrate isotopic heterogeneity within individual hand samples (i.e., on length scales of centimeters; Fig. 7). Analyses of single glass pieces from a single lava sample (“intra-sample” analyses) have ranges in $\delta^{18}O$ of up to ~0.8‰, and analyses of single olivine grains from a single lava sample have ranges in $\delta^{18}O$ of up to ~0.7‰ (compared to analytical uncertainty of ±0.15‰ for glass, ±0.24‰ for olivine; Table 3). For $\delta^{18}O_{gl}$, intra-sample variation is the least for summit samples (e.g., 1801-11 with single analyses having nearly identical $\delta^{18}O_{gl}$) and the most for rift samples (e.g., NRZ sample 156-6 has single analyses of $\delta^{18}O_{gl}$ ranging from 5.4 to 5.9‰ and SRZ sample 513-7A has single analyses of $\delta^{18}O_{gl}$ ranging from 5.1 to 5.6‰). For $\delta^{18}O_{ol}$, the NRZ and SRZ show comparable intra-sample variation (e.g., NRZ sample 156-6 has single analyses of $\delta^{18}O_{ol}$ ranging from 4.9 to 5.4‰ and SRZ sample 513-7A has single analyses of $\delta^{18}O_{ol}$ ranging from 4.5 to 5.2‰).

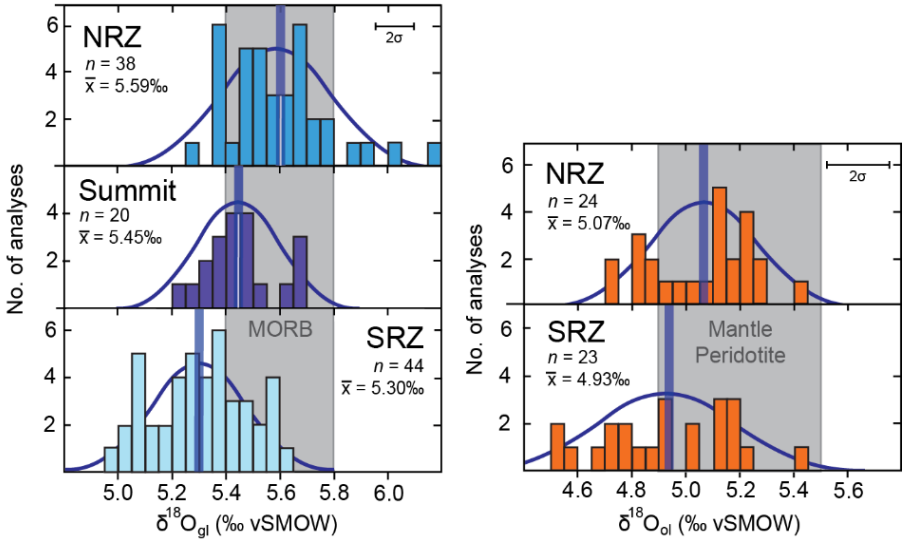

Figure 6. Single analyses of glass and olivine $\delta^{18}O$, categorized by region of the volcanic edifice. Line styles and fields described in caption of Fig. 5. Note that NRZ subsets are offset relatively high $\delta^{18}O$ values relative to SRZ subsets. Histogram bars are 0.05‰ wide.

Table 4. Results of statistical comparison of regional sample subsets of glass and olivine $\delta^{18}O$. All statistical tests were conducted at the significance level $\alpha = 0.05$. In this caption only, the term "sample" is used in a statistical context and refers to a group of collected measurements (e.g., all single analyses of glass in the NRZ constitute the NRZ glass sample). This is in contrast to the general use of "sample" when referring to individual hand sample lavas in the main text of this study. The one-sample Kolmogorov-Smirnov (K-S) Test reports a p-value equal to the probability of a given sample being drawn from a reference population distribution; in this case, a normal distribution (i.e., $p > 0.05$ suggests that a sample does not significantly deviate from a normal distribution). The two-tailed *t*-test for Independence of Samples reports a p-value equal to the probability that two samples are drawn from the same population (i.e., $p < 0.05$ suggests that the two samples being compared are drawn from statistically significantly distinct populations).
[a]This result is not statitistically significant at $\alpha = 0.05$; it is noted that it would be statitistically significant at $\alpha = 0.1$.
[b]The K-S Test is not statistically robust with low *n* (e.g., n = 4), so it cannot be executed on sample-averaged NRZ or SRZ olivine samples.
[c]The *t*-test is not statistically robust on comparisons of samples that cannot be assumed to have a normal distribution.

		Glass		**Olivine**	
Single Analyses	Kolmogorov-Smirnov Test of Normality	All	p = 0.97	All	p = 0.23
		NRZ	p = 0.81	NRZ	p = 0.42
		Summit	p = 0.92	SRZ	p = 0.89
		SRZ	p = 0.93		
	t-Test for Independence of Samples	NRZ vs. SRZ	p = <0.001	NRZ vs. SRZ	p = 0.032
		NRZ vs. Summit	p = 0.005		
		SRZ vs. Summit	p = 0.001		
Sample-Averaged Analyses	Kolmogorov-Smirnov Test of Normality	All	p = 0.78	All	p = 0.64
		NRZ	p = 0.89	*NRZ*[b]	~
		Summit	p = 0.79	*SRZ*[b]	~
		SRZ	p = 0.86		
	t-Test for Independence of Samples	NRZ vs. SRZ	p = <0.001	*NRZ vs. SRZ*[c]	~
		NRZ vs. Summit	p = 0.02		
		SRZ vs. Summit[a]	p = *0.07*		

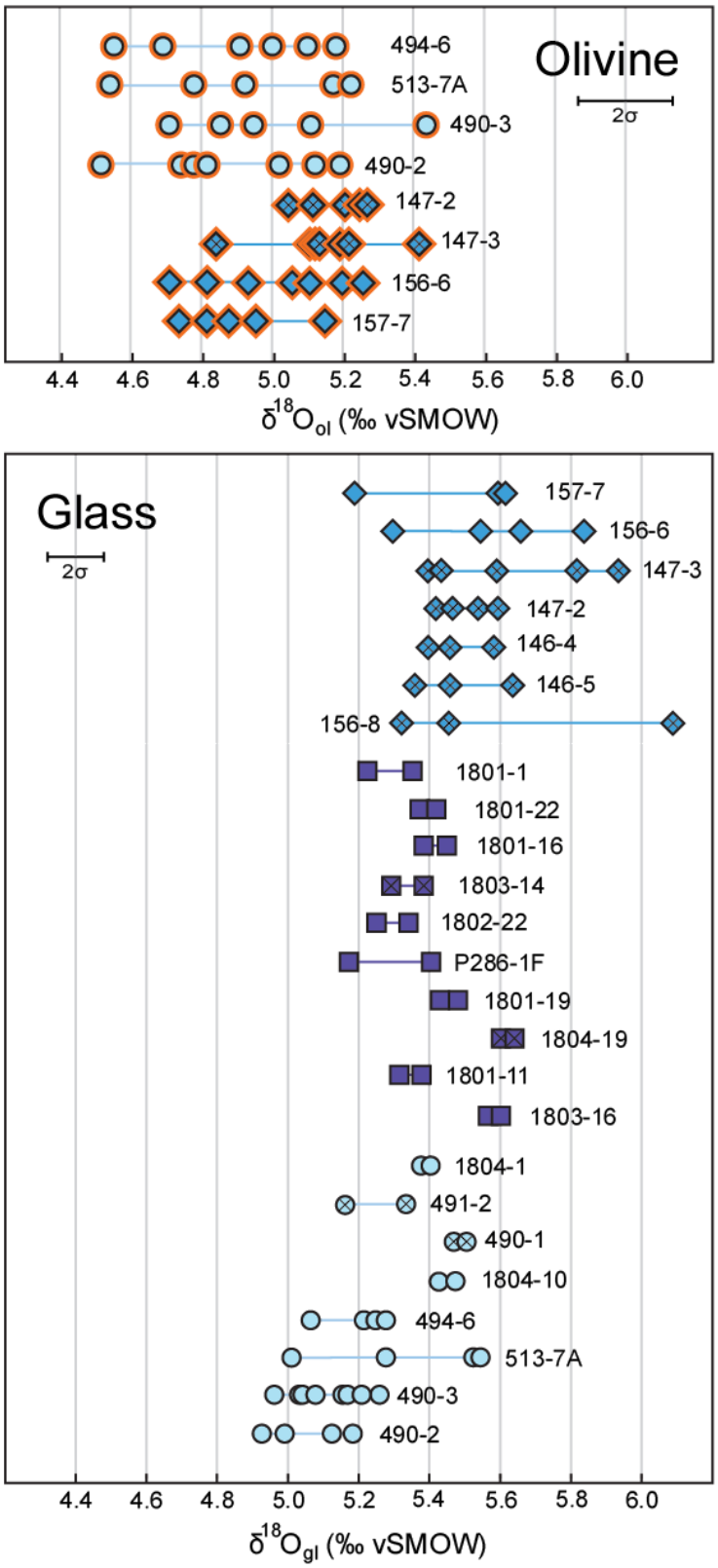

Figure 7. Intra-sample variation in glass and olivine $\delta^{18}O$ analyses. Single analyses of glass pieces and olivine grains from within single samples are heterogeneous beyond analytical uncertainty. Symbols described in Fig. 1.

3.4. GLASS STABLE H ISOTOPIC COMPOSITION

Glass δD ranges from -83 to -27‰ with an average of -69 ± 13‰ (Table 3). There is no evidence for hydrogen isotopic heterogeneity in the Kamaʻehu glasses based on replicate analyses of individual samples. The δD values cluster in two groups (Fig. 8). The relatively low δD group has an average of -73 ± 6‰ and the relatively high-δD group has an average of -30 ± 2‰. The low-δD group is similar to the global average of MORB (-75‰; Dixon et al., 2017).

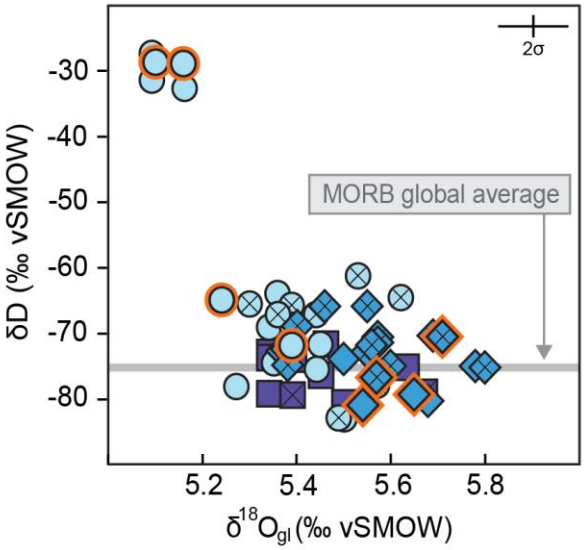

Figure 8. Sample-averaged $\delta^{18}O_{gl}$ vs. δD. δD values of Kamaʻehu glasses cluster around the mean value for globally distributed MORB (-75‰; Dixon et al., 2017). Five samples from the lower SRZ (Fig. 1) have relatively high δD. This high-δD group is only slightly lower in $\delta^{18}O$ than samples that do not have elevated δD.

4. DISCUSSION

The range of glass and olivine $\delta^{18}O$ values observed at Kamaʻehu Volcano broadly overlaps with the range of fresh MORB glass (5.4 to 5.8‰; Eiler et al., 2000; Eiler, 2001; Harmon &; Hoefs, 1995) and olivine in mantle peridotites (4.9 to 5.5‰; Mattey et al., 1994). This result confirms observations from Eiler et al. (1996a, b), Garcia et al. (1998a), and Wang et al. (2003) that lavas from many Hawaiian volcanoes have $\delta^{18}O_{ol}$ similar to the depleted upper mantle. The $\delta^{18}O_{gl}$ and $\delta^{18}O_{ol}$ values demonstrate systematic isotopic variation across the Kamaʻehu NRZ, summit, and SRZ. Significant variation also exists between single glass analyses and between single olivine analyses erupted in the same lava flow. Most glasses in this study have δD values (average δD = -68.7‰) comparable to that previously reported for Kamaʻehu glass (-73 ± 12‰; Loewen et al., 2019; Garcia et al., 1989) and overlapping with the range expected for Pacific MORB (-60 ± 5‰; Clog et al., 2013; Dixon et al., 2017). Altogether, the δD, $\delta^{18}O_{gl}$, and $\delta^{18}O_{ol}$ data presented in this study reveal the isotopic variation of Kamaʻehu magmas on a range of scales: 1) within individual lava samples, 2) across regions of the volcanic edifice, and 3) in the context of the Hawaiian mantle plume.

4.1. CRUSTAL PROCESSES AT KAMA‘EHU VOLCANO

4.1.1. O ISOTOPIC HETEROGENEITY WITHIN INDIVIDUAL SAMPLES

Forsterite content is useful for determining the relationship between olivine crystals and their host glass because olivine inherits its Fe-Mg composition from the surrounding melt by either growth or diffusive reequilibration (Roeder & Emslie, 1970; Dohmen & Chakraborty, 2007; Chakraborty et al., 2010). The analyzed olivine grains demonstrate crystal-glass Fe-Mg disequilibrium (Fig. 9), indicating that almost all of these olivine crystals are genetically unrelated (or at least indirectly related) to their host liquid. Furthermore, the compositions within an individual lava range widely in Fo (e.g., NRZ sample 490-2 has Fo_{77} to Fo_{91}; Fig. 4, Fig. 9). Thus, a single rising magma may incorporate olivine derived from many distinct parent magmas (e.g., Helz, 1987). The textural diversity of these phenocrysts is evident in backscatter electron (BSE) images, where some olivine grains demonstrate reverse and multi-stage zoning (Fig. 10).

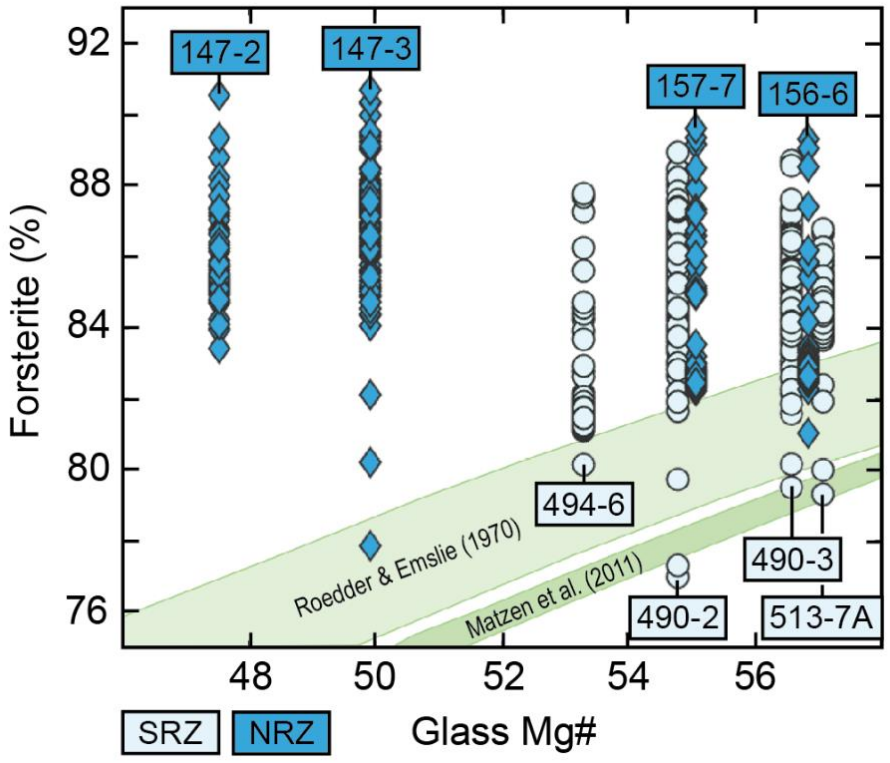

Figure 9. Glass Mg# vs. intra-sample distributions of olivine core forsterite content. Individual symbols represent single analyses of olivine core Fo. Equilibrium fields are given by Roeder & Emslie (1970; Fe-Mg K_D = 0.3 ±0.03) and Matzen et al. (2011; Fe-Mg K_D = 0.343 ± 0.008). Olivine-melt equilibrium is highly dependent on melt oxygen fugacity (Christie et al., 1986; Cottrell et al., 2017); Mg # is calculated assuming Fe^{2+}/Fe^{3+} = 0.17 based on analyses of undegassed olivine-hosted melt inclusions from Kīlauea (Helz et al., 2017). Olivine grains that plot outside of green fields are not in Fe-Mg equilibrium with their host glass.

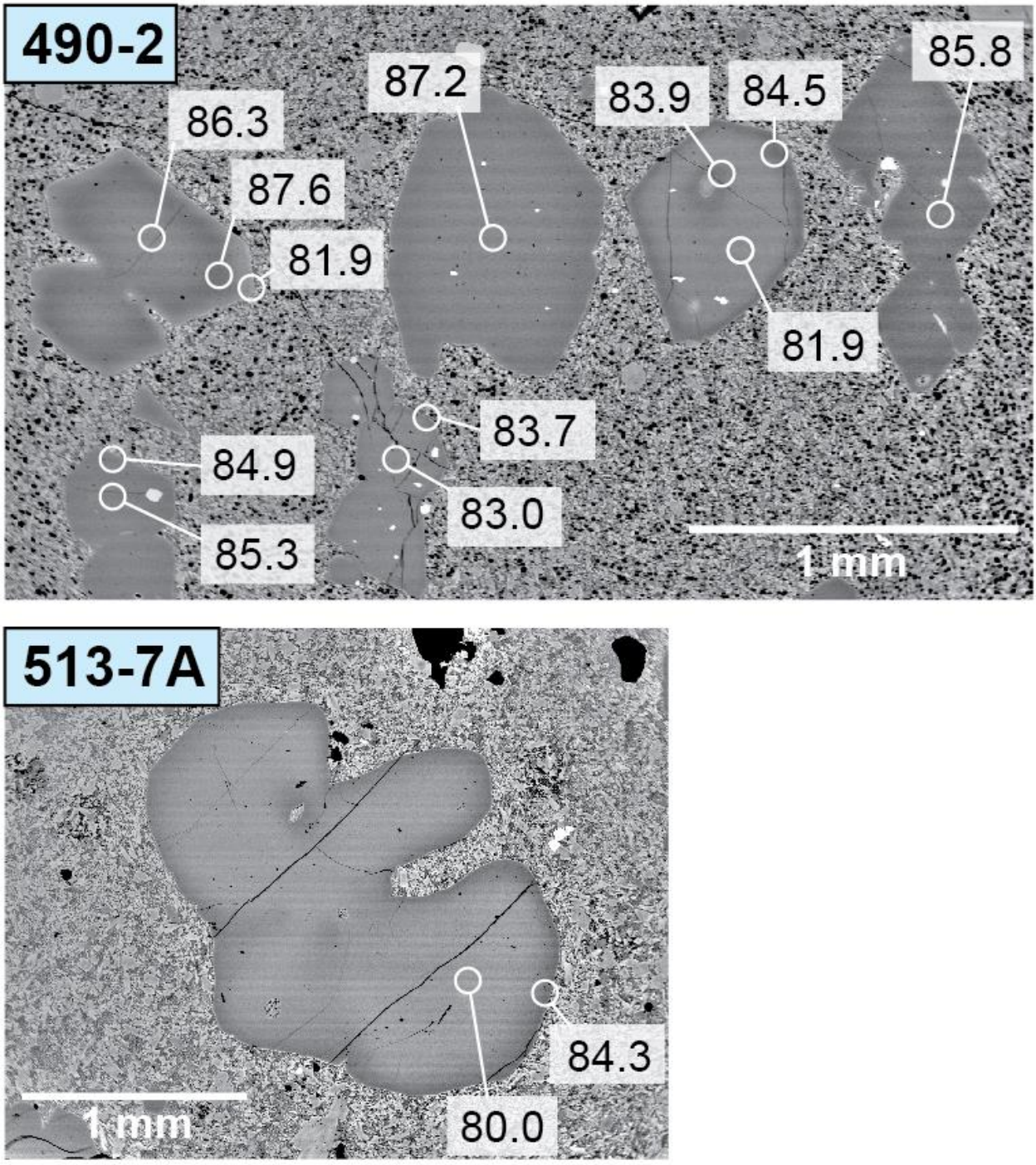

Figure 10. BSE images of olivine in thin section, annotated with core and rim Fo contents. Open circles represent single-spot electron microprobe analyses. Sample ID of pictured thin section listed in top left corner. Horizontal lines are an instrumental artifact of electron beam interference. Images were processed with a flat-field transformation using ImageJ software to ensure that grayscale values represent Fo values that are internally consistent for each image. Note rims of variable Fo content in phenocrysts adjacent to each other in thin section.

The textural complexity of olivine grains and their lack of Fe-Mg equilibrium with their host glass suggest that olivine has been physically separated from its parent melt and/or that the parent melt has shifted in composition after precipitating olivine. Olivine is expected to crystallize in isotopic equilibrium with its parent melt (Eiler, 2001), but this equilibrium will not be preserved in the erupted lava if subsequent processes isolate or alter the composition of either phase (e.g., Garcia et al., 1998a, 2008). In both the NRZ and SRZ, the $\Delta^{18}O_{gl\text{-}ol}$ values ($\delta^{18}O_{gl}$ - $\delta^{18}O_{ol}$) observed within individual samples is much greater than that expected from equilibrium fractionation (+0.4‰; Eiler, 2001). This result may be explained by entrainment of compositionally diverse olivine phenocrysts and incomplete mixing of variable-$\delta^{18}O$ melts, which would decouple liquid and crystals originally in isotopic equilibrium. These mechanisms would also cause $\delta^{18}O_{ol}$ and $\delta^{18}O_{gl}$ values that are highly variable on small length scales. Thus, intra-sample O isotopic heterogeneity and olivine-liquid disequilibrium may be attributed to olivine entrainment and lack of pre-eruptive melt homogenization in the shallow Kama‘ehu plumbing system.

4.1.2. ISOTOPIC HETEROGENEITY ACROSS THE VOLCANIC EDIFICE

Kama‘ehu magmas likely interact with seawater-altered or seawater-derived materials (Dixon & Clague, 2001) due to its submarine volcanic setting. Both hydrothermally concentrated brine and altered rock have been proposed as assimilants in the shallow Kama‘ehu plumbing system based on high Cl contents (Kent et al., 1999a, b; Dixon et al., 2001) and excess ^{234}U (Pietruszka et al., 2011) in fresh glasses. Incorporation of hydrothermally altered materials is also expected to influence $\delta^{18}O_{liq}$ and δD, although this effect has previously been interpreted as relatively insignificant (Garcia et al., 1989; Garcia et al., 1993; Eiler et al., 1996b).

Fluids in submarine hydrothermal systems are expected to have O and H isotopic compositions similar to seawater (~0‰; Shanks et al., 1995; Muehlenbachs, 1998) such that magmas assimilating these components will shift toward lower $\delta^{18}O$ and higher δD (e.g., Kyser & O’Neil, 1984; Eiler et al., 1996b). Assimilation of this seawater-derived fluid will also elevate Cl and H_2O concentrations (e.g., Michael & Schilling, 1989; Jambon et al., 1995), decoupling them from other elements that behave incompatibly during magmatic differentiation (e.g., K_2O, P_2O_5). The five SRZ samples with high δD values (~-30‰) are therefore likely to have assimilated hydrothermal fluids (e.g., Kent et al., 1999a, b) because these glasses demonstrate

high Cl/K_2O, high H_2O concentrations, and the lowest $\delta^{18}O_{gl}$ values in our dataset. The high H_2O contents of these glasses relative to other Kama‘ehu samples at a given MgO content (Fig. 3) are consistent with assimilation of a significant volume of fluid (e.g., Coombs et al., 2004). However, the $\delta^{18}O_{gl}$ values of these samples are only ~0.3‰ lower than the average $\delta^{18}O_{gl}$ value for all samples in this study (~5.4‰), and only 0.1‰ lower than the $\delta^{18}O_{gl}$ values of some samples with near-average (i.e., relatively uncontaminated) Cl/K_2O, H_2O content, and δD (Fig. 11). Thus, even instances of significant fluid assimilation negligibly affect $\delta^{18}O$ within analytical uncertainty (±0.15‰). A possible explanation is that parental magmas contain ~40 to 50 wt. % oxygen, which may dilute contamination, whereas hydrogen makes up less than a tenth of a wt. % (e.g., Table 1). This interpretation also explains the decoupling of $\delta^{18}O$ and δD in Kama‘ehu glasses, contrary to hypotheses that shallow assimilation may affect both isotopic signatures to a similar extent (e.g., Garcia et al., 1989). Accordingly, the assimilation process (or assimilant) that increases δD values, Cl/K_2O, and H_2O contents in the glass is likely different from the assimilation process that affects glass $\delta^{18}O$.

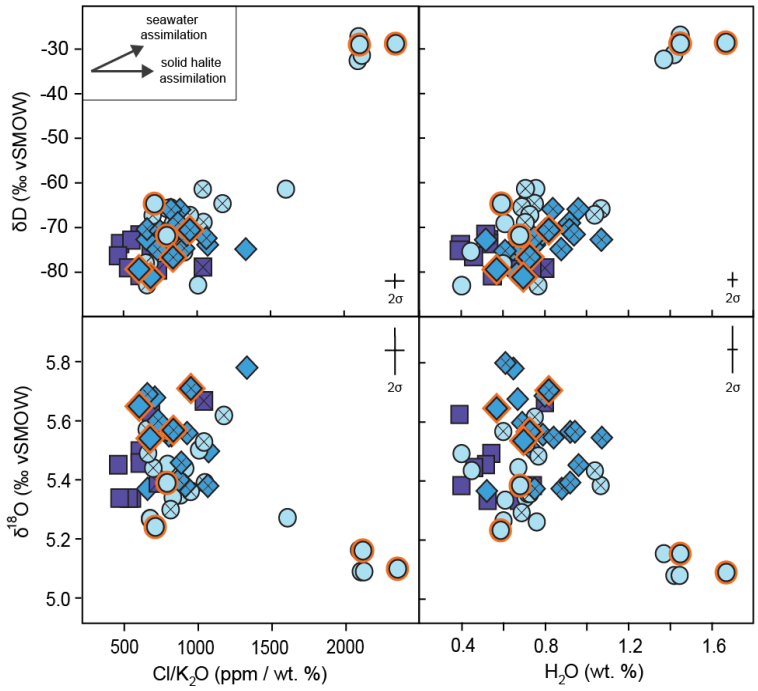

Figure 11. Bivariate diagrams of sample-averaged glass $\delta^{18}O$ and δD vs. Cl/K_2O and H_2O content. Five samples from the SRZ form a group of high-δD samples that are also anomalously enriched in Cl/K_2O and H_2O wt. %. Note that high-δD samples have $\delta^{18}O$ values that are relatively low, but not anomalously low. Samples that show elevated Cl/K_2O without corresponding high δD values and H_2O contents are more likely to have assimilated solid halite. Vectors for assimilation of seawater and halite taken from Loewen et al. (2019). Symbol descriptions given in Fig. 1.

Hydrothermal rock presents another potential assimilant that may alter magmatic $\delta^{18}O$ at Kama‘ehu (e.g., Wang et al., 2003, 2008). However, $\delta^{18}O_{gl}$ is not correlated with glass MgO contents in Kama‘ehu lavas (Fig. 12), as would be expected from AFC-driven shifts in melt composition. The absence of this relationship may be because rocks in the Kama‘ehu volcanic edifice are altered in a submarine setting. Submarine rocks have ample opportunity to participate in isotopic exchange with seawater, and the effects of this exchange on the composition of oceanic crust is well-studied (e.g., Muehlenbachs & Clayton, 1976; Gregory & Taylor, 1981; Alt et al., 1986; Staudigel et al., 1995; Alt et al., 2006). Submarine basalts may alter to $\delta^{18}O$ values above or below that of depleted upper mantle (~3 to 11‰; Gregory & Taylor, 1981; Alt et al., 2006) depending on the temperature at which they are altered: alteration at high temperatures (>250 °C) causes ^{18}O depletion, and alteration at low temperatures (<250 °C) causes ^{18}O enrichment (e.g., Alt et al., 2006). In contrast, rocks in subaerial environments are typically altered by groundwater derived from low-$\delta^{18}O$ meteoric water, causing those altered rocks to have $\delta^{18}O$ values equal to or below depleted upper mantle values (as low as ~1.9‰; e.g., Garcia et al., 2008). This key difference makes it difficult to apply models of differentiation-coupled $\delta^{18}O_{ol}$ variation (e.g., Wang & Eiler, 2008) to Kama‘ehu magmas because these models assume that assimilation causes magmatic $\delta^{18}O$ to vary unidirectionally from source compositions as AFC proceeds, which may not be appropriate for submarine systems. Thus, it is likely that assimilation of variably altered rock occurs within the Kama‘ehu shallow volcanic edifice, but this assimilation will not necessarily couple magmatic $\delta^{18}O$ with indicators of magmatic differentiation (e.g., glass MgO content).

Instead, it must be considered that the wide range of temperatures of hydrothermal fluids circulating within Kama‘ehu (~30 to >300 °C; Wheat et al., 2000) will cause rocks in the hydrothermal edifice to alter to variable $\delta^{18}O$ compositions, which may be lower or higher than the assumed $\delta^{18}O$ value of uncontaminated melts. Following the temperature-dependence of the $\delta^{18}O$ value of altered rock proposed by Alt et al. (2006), assimilation will cause decreases in $\delta^{18}O$ in regions exhibiting high vent temperatures (and therefore low $\delta^{18}O_{altered\ rock}$) and increases in magmatic $\delta^{18}O$ in regions exhibiting low vent temperatures (and therefore high $\delta^{18}O_{altered\ rock}$). The statistically significant differences in regional isotopic composition observed in Kama‘ehu samples may then be explained if (1) relative ^{18}O enrichment in NRZ magmas corresponds to circulation of predominantly low-T (<250 °C) fluids in the NRZ, (2) relative ^{18}O depletion in

SRZ magmas corresponds to circulation of predominantly high-T (>250 °C) fluids in the SRZ, and (3) MORB-like $\delta^{18}O$ values in the summit region correspond to circulation of both high- and low-T fluids in similar proportions over time in the summit region. This theory is supported by independent observations of vigorous hydrothermal venting in the summit and SRZ (Malahoff et al., 1982; Karl et al., 1988; Lō‘ihi Science Team, 1997) and the conclusion of Wheat et al. (2000) that hydrothermal fluids within the Kama‘ehu volcanic edifice contain both a high- and low-T component.

Alternatively, the intermediate $\delta^{18}O$ values and limited intra-sample variation of lavas from the summit region (Fig. 7) may reflect characteristics of the Kama‘ehu magmatic plumbing system. If a magma reservoir has a relatively high rate of magma supply, then the mass of fresh magma will tend to be much greater than the mass of assimilant incorporated into the magma, effectively diluting the effects of shallow assimilation on magmatic $\delta^{18}O$. Conversely, reservoirs with relatively low rates of magma supply are expected to stall and undergo AFC, increasing the proportional contribution of the assimilant to $\delta^{18}O_{liq}$ (e.g., Gaffney et al., 2004). At Hawaiian volcanoes, rift zones primarily receive magma from the summit reservoir and thus are likely to contain disconnected “pockets” of stagnating magma (e.g., Shamberger & Garcia, 2007; Pietruszka et al., 2018), which may be more susceptible to assimilation-forced shifts to relatively high- or low-$\delta^{18}O$ compositions. This idea is comparable to the interpretation that magmas in transit down rift zones may have more time to participate in isotopic exchange with hydrothermally altered wall rock, as observed for Pu‘u‘ō‘ō lavas at Kīlauea (Garcia et al., 1998a). In contrast, sub-summit reservoirs are expected to receive frequent and direct deliveries of magma from the mantle (e.g., Clague et al., 1987, Pietruszka et al., 2015), which may dilute the influence of assimilation on $\delta^{18}O_{liq}$ (e.g., Gaffney et al., 2004) and produce relatively uncontaminated, intermediate-$\delta^{18}O$ summit lavas. Moreover, high rates of magma supply correspond to larger, more stable, and more interconnected reservoirs over time (Clague et al., 1987; Swanson et al., 2014; Lynn et al., 2017), which are more likely to homogenize prior to eruption (e.g., Pietruszka et al., 2015). A greater potential for homogenization may explain why summit lavas demonstrate lower intra-sample heterogeneity (e.g., maximum range in single $\delta^{18}O_{gl}$ analyses within a single lava = ~0.2‰) than lavas from the NRZ or SRZ (maximum range in single $\delta^{18}O_{gl}$ analyses within a single lava = ~0.8‰). To emphasize this point, it is noted that the summit sample with maximum intra-sample variation (P286-1F; $\delta^{18}O_{gl}$ = 5.2 to 5.4‰) was

erupted in association with the 1996 caldera collapse (Garcia et al., 1998b; Rubin et al., 2005). Caldera collapses disrupt the summit plumbing system and are expected to limit homogenization of its magma reservoirs (e.g., Garcia et al., 2008; Lynn et al., 2017); yet, this sample still demonstrates lower degrees of intra-sample heterogeneity than most samples erupted along rift zones. In summary, the intermediate $\delta^{18}O_{gl}$ values and low intra-sample heterogeneity of summit lavas may be related to the comparatively high magma supply to the summit region. Variations in $\delta^{18}O_{ol}$ and $\delta^{18}O_{gl}$ for Kama‘ehu lavas may thus be controlled by processes operating within the shallow volcanic edifice. However, repeated analyses of $\delta^{18}O$ in glass and olivine from many lavas may potentially be used to characterize isotopic composition of the Kama‘ehu mantle source and its primary magmas.

4.2. O & H ISOTOPIC COMPOSITION OF THE KAMA‘EHU MANTLE SOURCE

The δD, $\delta^{18}O_{gl}$, and $\delta^{18}O_{gl}$ datasets presented in this study have mean values generally comparable to those expected from melting of peridotitic mantle (Kyser & O’Neil, 1984; Mattey et al., 1994; Eiler et al., 2001). Previous studies have noted the coexistence of upper mantle-like stable isotopic compositions with high $^{3}He/^{4}He$ in Kama‘ehu lavas, suggesting that the Kama‘ehu mantle source is depleted in radiogenic isotope composition (e.g., relatively low $^{87}Sr/^{86}Sr$ and high εNd), MORB-like in $\delta^{18}O_{ol}$ (e.g., $\delta^{18}O_{ol} = 5.2‰$; Eiler et al., 1996a), and similar to primordial mantle based on δD values (Loewen et al., 2019). The agreement of many ($n = 63$) δD analyses from this study with these reported values (except for samples clearly contaminated by seawater-derived components; Fig. 11) favors previous interpretations that the Kama‘ehu mantle source has an H isotopic composition of ~-73 ± 6‰.

Source O isotopic composition, however, is more difficult to decipher because it is influenced by magmatic processes within the volcanic edifice and is likely to be decoupled from δD. A source control on magmatic $\delta^{18}O$ at Hawaiian volcanoes has been proposed based on correlations between $\delta^{18}O_{ol}$ and Pb-Nd-Sr-Os radiogenic isotope and/or incompatible trace element ratios (Eiler et al., 1996a; Lassiter & Hauri, 1998; Wang et al., 2010). These models do not detail the variation expected within an individual volcano, but they do suggest that mean $\delta^{18}O_{ol}$ is a reasonable estimator of source $\delta^{18}O_{liq}$. Following this assumption, the $\delta^{18}O_{liq}$ of Kama‘ehu parent melts is ~5.4‰ (assuming an equilibrium fractionation of +0.4‰; Eiler, 2001). Notably, this $\delta^{18}O_{liq}$ value is higher than the source composition that proposed by Garcia et al.

(5.0 to 5.1‰;1989) and lower than that proposed by Eiler et al. (~5.6‰; 1996). Yet, this result is reasonable because Kama‘ehu is expected to have a source with a significant component of depleted peridotite (Garcia et al., 1993, 1995; Pietruszka et al., 2013), and remarkable because the $\delta^{18}O_{gl}$ dataset precisely reproduces this value (mean $\delta^{18}O_{gl} = 5.4 \pm 0.2$‰; Table 3). Thus, assimilation of both high- and low-$\delta^{18}O$ components may buffer mean $\delta^{18}O_{liq}$, such that Kama‘ehu olivine *and* glass reflect source-derived O isotopic compositions when averaged over many samples from many parts of the volcanic edifice.

Magma compositions at neighboring Mauna Loa and Kīlauea fluctuate consistently due to melting of small-scale heterogeneities in the Hawaiian plume (Pietruszka & Garcia, 1999; Marske et al., 2007). If these heterogeneities represent blobs of an ancient, variably dehydrated slab entrained in the Hawaiian plume (e.g., Pietruszka et al., 2013), then it would not be surprising for similar fluctuations to develop in $\delta^{18}O$ of parent melts at these volcanoes. If melting of a heterogeneous source were to dominate $\delta^{18}O$ variation, $\delta^{18}O_{ol}$ and/or $\delta^{18}O_{gl}$ would correlate with other geochemical indicators of mantle provenance, such as ratios of incompatible elements (e.g., K_2O/TiO_2). Though a correlation between $\delta^{18}O_{gl}$ and K_2O/TiO_2 is not observed in Kama‘ehu glasses (Fig. 12), it is possible that this relationship has been obscured by crustal

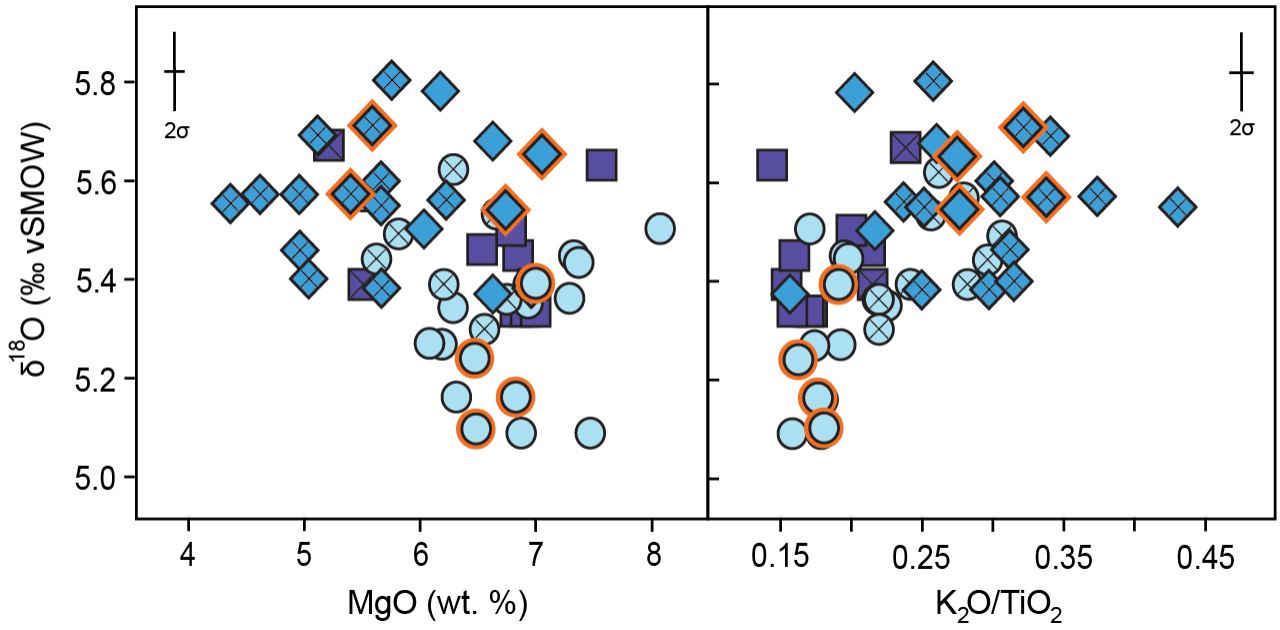

Figure 12. Bivariate diagrams of sample-averaged glass $\delta^{18}O$ vs. K_2O/TiO_2 and MgO content. $\delta^{18}O_{gl}$ does not show any correlation with geochemical tracers of magmatic differentiation (MgO wt. %) or mantle provenance (K_2O/TiO_2). Symbol descriptions in Fig. 1.

contamination in the shallow volcanic edifice. Indeed, self-assimilation has been shown to overprint source-derived compositional variation in $\delta^{18}O_{ol}$ and $\delta^{18}O_{gl}$ at many individual Hawaiian volcanoes (e.g., Wang et al., 2008; Garcia et al., 1998a, 2008; Lassiter et al., 2022). An example of this overprinting at Kama‘ehu is the distinct $\delta^{18}O$ values of magmas erupted in each region of the volcanic edifice. It is improbable that these variations are source-derived because this idea would require that all magmas of a given initial composition take a predetermined path to the surface (i.e., all high-$\delta^{18}O$ magmas *must* erupt on the NRZ). Instead, it is more likely that magmas acquired distinct compositions within each region of the shallow magmatic plumbing system. Thus, strong assimilation signatures in Kama‘ehu lavas confirm the influence of crustal processes on magmatic $\delta^{18}O$, but do not eliminate the possibility of source contributions to lava O isotopic variation. For this reason, we propose that the Kama‘ehu mantle source has a mean of 5.4‰, but it is possible that individual batches of parental melt may vary both above or below this central value.

4.3. O ISOTOPIC MODEL OF THE KAMA‘EHU MAGMATIC PLUMBING SYSTEM

4.2.1. MODEL PART A

Parent magmas ascend into the shallow magmatic plumbing system with $\delta^{18}O_{liq}$ = ~5.4‰ and δD = ~-73‰. Mean $\delta^{18}O_{ol}$, $\delta^{18}O_{liq}$, and δD of Kama‘ehu magmas are derived from melting of the mantle source in the Hawaiian plume, which gives them O and H isotopic compositions similar to MORB. Some isotopic variation may be introduced to parent melts by entrainment of oceanic crust (Eiler et al., 1996a; Lassiter & Hauri, 1998; Wang et al., 2010; Gaffney et al., 2004). However, this variation may be insignificant or obscured by shallow magmatic processes because no correlation exists between $\delta^{18}O_{ol}$, $\delta^{18}O_{gl}$, and/or δD with geochemical tracers controlled by variable melting of a heterogeneous mantle source (e.g., K_2O/TiO_2).

4.2.2. MODEL PART B

Assimilation of variable-$\delta^{18}O$ and, in some instances, variable-δD components shifts magmatic O and H isotopic compositions away from their source-derived values. The large range of $\delta^{18}O$ and δD values observed in Kama‘ehu lavas is attributed to assimilation of fluid or variably altered materials in the volcanic edifice. Five SRZ samples demonstrate unambiguously elevated δD, Cl/K_2O, and water content, suggesting that their magmas incorporated seawater-derived

brines (e.g., Kent et al., 1999a, b; Dixon & Clague, 2001). The $\delta^{18}O_{gl}$ values of these samples are not significantly distinct from lavas having average δD, Cl/K_2O, and H_2O concentrations, indicating that $\delta^{18}O$ and δD are broadly decoupled in Kama‘ehu melts. Additionally, average $\delta^{18}O_{gl}$ varies systematically between the NRZ, summit, and SRZ. This variation is attributed to magmatic assimilation of altered basalt, which will vary in $\delta^{18}O$ depending on the temperature at which it is altered by circulating fluid (Alt et al., 2006). Thus, predominantly high-T hydrothermal alteration in the SRZ may produce relatively low-$\delta^{18}O$ assimilants, which decrease $\delta^{18}O_{liq}$ in contaminated magmas; and predominantly low-T alteration in the NRZ may produce relatively high-$\delta^{18}O$ assimilants, which increase $\delta^{18}O_{liq}$ in contaminated magmas. In the summit region, circulation of high- and low-T fluids may produce intermediate-$\delta^{18}O$ assimilants, and high magma supply rates may limit the influence of contamination on summit magmas (e.g., Gaffney et al., 2004).

4.2.3. MODEL PART C

Assimilation processes begin before/during fractional crystallization of olivine, causing $\delta^{18}O_{ol}$ to track with changing $\delta^{18}O_{liq}$. Like $\delta^{18}O_{gl}$, mean $\delta^{18}O_{ol}$ of NRZ lavas is higher than mean $\delta^{18}O_{ol}$ of SRZ lavas and the mean of $\delta^{18}O_{ol}$ from each region is distinct. The $\delta^{18}O$ value of olivine is expected to vary with the $\delta^{18}O$ of its host melt; if the melt is contaminated, olivine crystallizing in isotopic equilibrium with that melt will be similarly contaminated. The approximate coupling of average $\delta^{18}O_{ol}$ and $\delta^{18}O_{gl}$ within individual regions of the Kama‘ehu volcanic edifice therefore suggest that melts are contaminated prior to or during fractionation of at least some olivine (c.f., Garcia et al., 2008). The $\delta^{18}O$ value of altered rock in the volcanic edifice is too variable to produce correlations between indicators of magmatic differentiation (e.g., glass MgO content) and $\delta^{18}O_{gl}$, which precludes a first-order control of AFC processes on glass and olivine $\delta^{18}O$ (e.g., Wang & Eiler, 2008).

4.2.4. MODEL PART D

Olivine entrainment decouples $\delta^{18}O_{ol}$ and $\delta^{18}O_{gl}$ within individual lavas. Individual Kama‘ehu lavas contain olivine with a wide range in Fo contents, indicating that these crystals originated from melts of diverse Fe-Mg compositions (Roeder & Emslie, 1970). Moreover, the majority of phenocrysts in a given sample exhibit Fe-Mg disequilibrium with their host glass. These

observations provide evidence that olivine crystals are commonly transported to the surface by magmas with which they are not genetically related (e.g., Helz, 1987). Olivine populations will already have significant heterogeneity due to crystallizing from variably contaminated liquids; olivine entrainment amplifies this heterogeneity by placing crystals of unrelated origin in the same erupting melt. This process prevents individual lavas from demonstrating differences in $\delta^{18}O_{ol}$ and $\delta^{18}O_{liq}$ consistent with isotopic equilibrium except by coincidence.

4.2.5. MODEL PART E.

Melts erupt before significant homogenization can take place. Quenched glass in many lavas from the SRZ and NRZ preserve significant variations in $\delta^{18}O_{liq}$ on small length scales (i.e., centimeters). Some of these samples also demonstrate olivine grains with complex zoning patterns that may be distinct from those of immediately adjacent phenocrysts, which is consistent with the interaction of melts having contrasting Fe-Mg compositions and diverse crystal cargo (e.g., Helz, 1987). In contrast, lavas erupted in the summit region demonstrate limited intra-sample heterogeneity in $\delta^{18}O_{gl}$, possibly because a relatively high rate of magma supply favors reservoir interconnectedness, and therefore more thorough mixing (e.g., Pietruszka et al., 2015). The range of $\delta^{18}O$ values observed in individual lavas may be derived from assimilation of variable-$\delta^{18}O$ components and mitigated by the degree of homogenization prior to eruption.

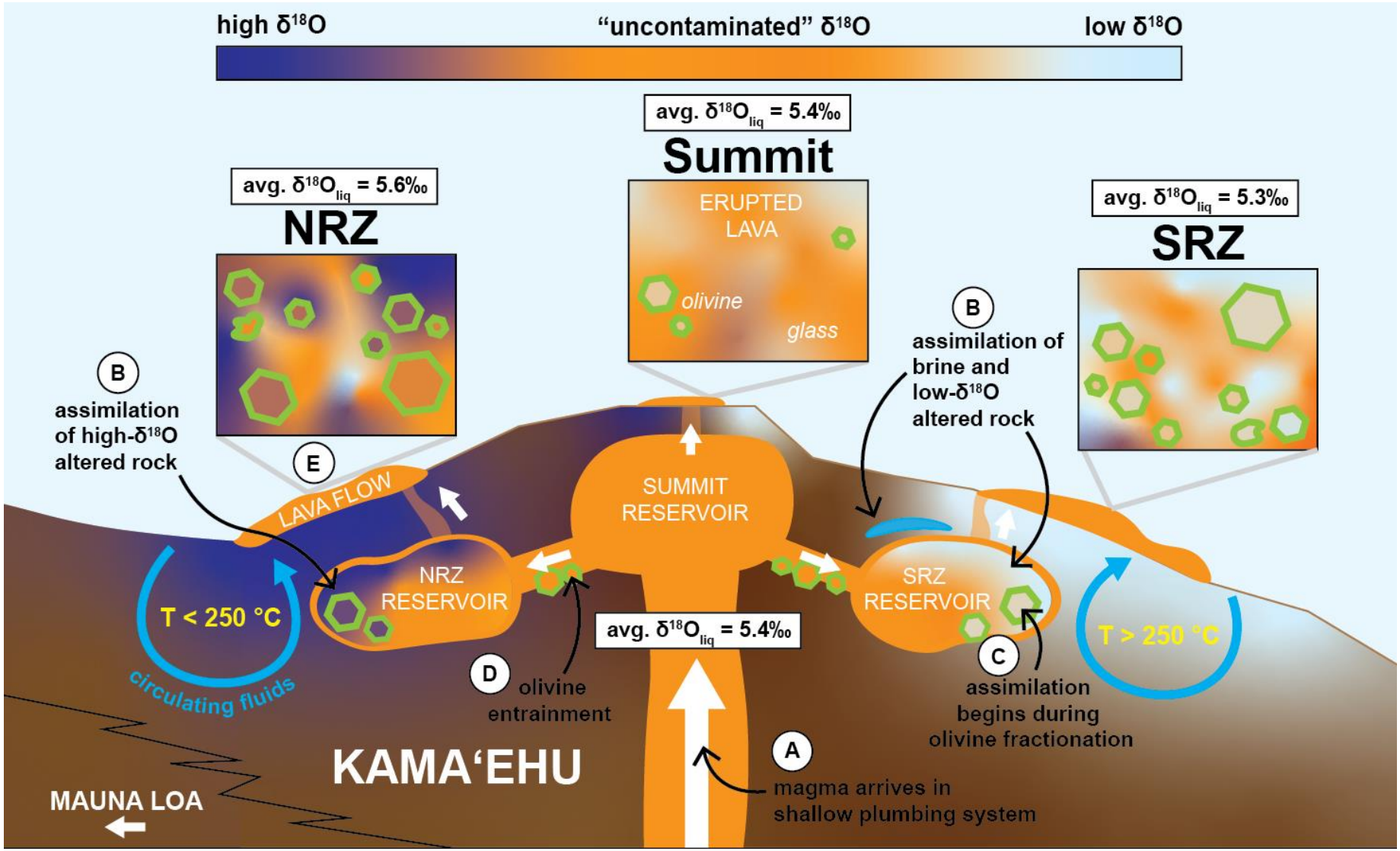

Figure 13. Model of Kama'ehu shallow volcanic plumbing system, consistent with O and H isotopic evidence. Schematic diagram showing cross section of Kama'ehu plumbing system, facing east. White arrows indicate paths of magma movement. Processes detailed in section 4.3.

4. CONCLUSION & BROADER IMPLICATIONS

A dataset of complementary $\delta^{18}O_{gl}$, $\delta^{18}O_{ol}$ and δD analyses reveals an isotopic portrait of Kama‘ehu Volcano on a variety of scales. Melts of the Kama‘ehu mantle source region likely have a mean composition of $\delta^{18}O_{liq} = 5.4 \pm 0.2‰$ and $\delta D = -73 \pm 6‰$, similar to MORB. Individual batches of melt may vary above or below these values due to heterogeneities in the Kama‘ehu mantle source. We find that magmas generally retain their mantle-derived H isotopic signature until eruption, except in the rare case of contamination by seawater-derived brines. Assimilation of these fluids may slightly influence $\delta^{18}O$, but magmatic O and H isotopic compositions are decoupled due to assimilation of altered, variable-$\delta^{18}O$ rock within the volcanic edifice. The $\delta^{18}O$ of altered basalt is a function of the temperature at which it is altered, so the composition of an assimilant is highly dependent on properties of the regional hydrothermal system. This process leads to the eruption of isotopically distinct magmas in each region of the volcanic edifice: (1) NRZ magmas may assimilate ^{18}O-enriched rocks altered at predominantly low T (<250 °C), (2) SRZ magmas may assimilate ^{18}Odepleted rocks altered at predominantly high T (>250 °C), and (3) magmas in the summit region may assimilate rocks altered at high and low temperatures in similar proportions, so its erupted lavas have $\delta^{18}O$ similar to MORB. Furthermore, relatively high rates of magma supply to the summit reservoir system may limit the effects of assimilation on $\delta^{18}O$ of lavas erupted in the summit region. For $\delta^{18}O_{ol}$ and $\delta^{18}O_{gl}$, heterogeneity within individual regions is attributed to the spatial and temporal variability of hydrothermal and assimilation processes. This heterogeneity is amplified by olivine entrainment and, possibly, shallow interaction of compositionally distinct melts prior to or during eruption of individual lava flows.

These conclusions present strong evidence that variation in $\delta^{18}O$ of lavas at individual Hawaiian volcanoes is significantly affected by shallow magmatic processes, which obscures but does not preclude contributions of source-derived variation in magmatic $\delta^{18}O$. It is thus necessary to collect O isotopic analyses of many (e.g., $n > 50$) samples in order to constrain the effects of these processes and determine signatures that are truly representative of the mantle source. Separately, we find that most erupted glasses at Kama‘ehu appear to preserve their source-derived H isotopic compositions, and that H_2O of most glasses is coupled with other incompatible elements. Thus, the δD and H_2O dataset in this study present an exciting future opportunity to infer the concentration of water in Kama‘ehu mantle source.

REFERENCES CITED

Alt, J. C., Muehlenbachs, K., & Honnorez, J. (1986). An oxygen isotopic profile through the upper kilometer of the oceanic crust, DSDP Hole 504B. *Earth and Planetary Science Letters*, *80*(3-4), 217–229. doi:10.1016/0012-821x(86)90106-8.

Alt, J. C., and Bach, W. (2006). Oxygen isotope composition of a section of lower oceanic crust, ODP Hole 735B, *Geochemistry, Geophysics, Geosystems*, *7*, Q12008.

Bindeman, I. N., Sigmarsson, O., & Eiler, J. (2006). Time constraints on the origin of large volume basalts derived from O-isotope and trace element mineral zoning and U-series disequilibria in the Laki and Grímsvötn volcanic system. *Earth and Planetary Science Letters*, *245*(1-2), 245-259.

Bindeman, I., Gurenko, A., Carley, T., Miller, C., Martin, E., & Sigmarsson, O. (2012). Silicic magma petrogenesis in Iceland by remelting of hydrothermally altered crust based on oxygen isotope diversity and disequilibria between zircon and magma with implications for MORB. *Terra Nova*, *24*(3), 227-232.

Bindeman, I. N., Greber, N. D., Melnik, O. E., Artyomova, A. S., Utkin, I. S., Karlstrom, L., & Colón, D. P. (2020). Pervasive hydrothermal events associated with large igneous provinces documented by the Columbia River Basaltic Province. *Scientific reports*, *10*(1), 1-9.

MacDonald, G.A. and Katsura, I. (1964) Chemical Composition of Hawaiian Lavas. Journal of Petrology, 5, 82-133.

Chakraborty, S. (2010). Diffusion coefficients in olivine, wadsleyite and ringwoodite. *Reviews in mineralogy and geochemistry*, *72*(1), 603-639.

Christie, D. M., Carmichael, I. S., & Langmuir, C. H. (1986). Oxidation states of mid-ocean ridge basalt glasses. *Earth and Planetary Science Letters*, *79*(3-4), 397-411.

Clague, D. A. (1987). Hawaiian xenolith populations, magma supply rates, and development of magma chambers. *Bulletin of Volcanology*, *49*(4), 577-587.

Clague, D. A., Paduan, J. B., Caress, D. W., Moyer, C. L., Glazer, B. T., & Yoerger, D. R. (2019). Structure of Lō ʻihi Seamount, Hawai ʻi and Lava flow morphology from high-resolution mapping. *Frontiers in Earth Science*, *7*, 58.

Clog, M., Aubaud, C., Cartigny, P., & Dosso, L. (2013). The hydrogen isotopic composition and water content of southern Pacific MORB: A reassessment of the D/H ratio of the depleted mantle reservoir. *Earth and Planetary Science Letters*, *381*, 156-165.

Coombs, M. L., Sisson, T. W., & Kimura, J. I. (2004). Ultra-high chlorine in submarine Kılauea glasses: evidence for direct assimilation of brine by magma. *Earth and Planetary Science Letters*, *217*(3-4), 297-313.

Cottrell, E., Birner, S. K., Brounce, M., Davis, F. A., Waters, L. E., & Kelley, K. A. (2021). Oxygen fugacity across tectonic settings. *Magma redox geochemistry*, 33-61.

Craig, H., & Lupton, J. E. (1976). Primordial neon, helium, and hydrogen in oceanic basalts. *Earth and Planetary Science Letters*, *31*(3), 369-385.

Dixon, J. E., & Clague, D. A. (2001). Volatiles in basaltic glasses from Loihi Seamount, Hawaii: Evidence for a relatively dry plume component. *Journal of Petrology*, *42*(3), 627-654.

Dixon, J. E., Bindeman, I. N., Kingsley, R. H., Simons, K. K., Le Roux, P. J., Hajewski, T. R., ... & Wallace, P. J. (2017). Light stable isotopic compositions of enriched mantle sources: Resolving the dehydration paradox. *Geochemistry, Geophysics, Geosystems*, *18*(11), 3801-3839.

Dohmen, R., & Chakraborty, S. (2007). Fe–Mg diffusion in olivine II: point defect chemistry, change of diffusion mechanisms and a model for calculation of diffusion coefficients in natural olivine. *Physics and Chemistry of Minerals*, *34*(6), 409-430.

Donovan, J. J., & Tingle, T. N. (1996). An improved mean atomic number background correction for quantitative microanalysis. *Microscopy and Microanalysis*, *2*(1), 1-7.

Eiler, J. M., Farley, K. A., Valley, J. W., Hofmann, A. W., & Stolper, E. M. (1996). Oxygen isotope constraints on the sources of Hawaiian volcanism. *Earth and Planetary Science Letters, 144(3-4),* 453–467.

Eiler J.M., Valley, J.W., Stolper, E.M., (1996a). Oxygen isotope ratios in olivine from the Hawaii scientific drilling project. *Journal of Geophysical Research, 101*(11), 807-11, 814.

Eiler, J.M., Schiano, P., Kitchen, N., Stolper, E.M., (2000b). Oxygen isotope evidence for recycled crust in the sources of mid ocean ridge basalts. *Nature, 403,* 530-534.

Eiler, J.M. (2001). Oxygen isotope variations of basaltic lavas and upper mantle rocks, *Reviews in Mineralogy & Geochemistry, 43,* 319–364.

Fornari, D. J., Garcia, M. O., Tyce, R. C., & Gallo, D. G. (1988). Morphology and structure of Loihi Seamount based on Seabeam sonar mapping. *Journal of Geophysical Research: Solid Earth*, *93*(B12), 15227-15238.

Gaffney, A. M., Nelson, B. K., Reisberg, L., & Eiler, J. (2004). Oxygen–osmium isotope systematics of West Maui lavas: A record of shallow-level magmatic processes. *Earth and Planetary Science Letters, 239(1-2),* 122–139.

Gao, R., Lassiter, J. C., Barnes, J. D., Clague, D. A., & Bohrson, W. A. (2016). Geochemical investigation of gabbroic xenoliths from Hualalai volcano: Implications for lower oceanic crust accretion and Hualalai Volcano magma storage system. *Earth and Planetary Science Letters*, *442*, 162-172.

Garcia, M. O., Muenow, D. W., Aggrey, K. E., & O'Neil, J. R. (1989). Major element, volatile, and stable isotope geochemistry of Hawaiian submarine tholeiitic glasses. *Journal of Geophysical Research: Solid Earth*, *94*(B8), 10525-10538.

Garcia, M. O., Jorgenson, B. A., Mahoney, J. J., Ito, E., & Irving, A. J. (1993). An evaluation of temporal geochemical evolution of Loihi summit lavas: results from Alvin submersible dives. *Journal of Geophysical Research: Solid Earth*, *98*(B1), 537-550.

Garcia, M.O., Pietruszka, A.J., Rhodes, J.M. (2003). A petrologic perspective of Kīlauea Volcano's Summit Magma Reservoir. *Journal of Petrology, 44, (12)*2313-2339.

Garcia, M. O., Ito, E., & Eiler, J. M. (2008). Oxygen Isotope Evidence for Chemical Interaction of Kīlauea Historical Magmas with Basement Rocks. *Journal of Petrology*, *49*(4), 757-769.

Garcia, M. O., Ito, E., Eiler, J. M., & Pietruszka, A. J. (1998). Crustal Contamination of Kilauea Volcano Magmas Revealed by Oxygen Isotope Analyses of Glass and Olivine fromPuu Oo Eruption Lavas. *Journal of Petrology*, *39*(5), 803-817.

Garcia, M. O., Rubin, K. H., Norman, M. D., Rhodes, J. M., Graham, D. W., Muenow, D. W., & Spencer, K. (1998). Petrology and geochronology of basalt breccia from the 1996 earthquake swarm of Loihi seamount, Hawaii: magmatic history of its 1996 eruption. *Bulletin of Volcanology*, *59*(8), 577-592.

Gregory, R. T., & Taylor Jr, H. P. (1981). An oxygen isotope profile in a section of Cretaceous oceanic crust, Samail Ophiolite, Oman: Evidence for δ18O buffering of the oceans by deep (> 5 km) seawater-hydrothermal circulation at mid-ocean ridges. *Journal of Geophysical Research: Solid Earth*, *86*(B4), 2737-2755.

Harmon, R.S., Hoefs, J. (1995). Oxygen isotope heterogeneity of the mantle deduced from global ^{18}O systematics of basalts from different geotectonic settings. *Contributions to Mineralogy & Petrology, 120,* 95-114.

Helz, R. T., (1987). Diverse olivine types in lava of the 1959 eruption of Kīlauea Volcano and their bearing on eruption dynamics. In: Decker, R.W., Wright, T.L., Stauffer, P.H., (eds) Volcanism in Hawai'i. US Geological Survey, Washington, DC, pp. 691-722.

Helz, R. T., Cottrell, E., Brounce, M. N., & Kelley, K. A. (2017). Olivine-melt relationships and syneruptive redox variations in the 1959 eruption of Kīlauea Volcano as revealed by XANES. *Journal of Volcanology and Geothermal Research*, *333*, 1-14.

Jambon, A., Déruelle, B., Dreibus, G., & Pineau, F. (1995). Chlorine and bromine abundance in MORB: the contrasting behaviour of the Mid-Atlantic Ridge and East Pacific Rise and implications for chlorine geodynamic cycle. *Chemical Geology*, *126*(2), 101-117.

Jarosewich, E., Parkes, A. S., & Wiggins, L. B. (1979). Microprobe analyses of four natural glasses and one mineral: an interlaboratory study of precision and accuracy. *Smithsonian contributions to the earth sciences*, *22*, 53-67.

Jarosewich, E., Nelen, J. A., & Norberg, J. A. (1980). Electron microprobe reference samples for mineral analyses. *Smithsonian contributions to the earth sciences*, *22*, 68-72.

Karl, D. M., McMurtry, G. M., Malahoff, A., & Garcia, M. O. (1988). Loihi Seamount, Hawaii: a mid-plate volcano with a distinctive hydrothermal system. *Nature*, *335*(6190), 532-535.

Kent, A. J., Clague, D. A., Honda, M., Stolper, E. M., Hutcheon, I. D., & Norman, M. D. (1999a). Widespread assimilation of a seawater-derived component at Loihi Seamount, Hawaii. *Geochimica et Cosmochimica Acta*, *63*(18), 2749-2761.

Kent, A. J., Norman, M. D., Hutcheon, I. D., & Stolper, E. M. (1999b). Assimilation of seawater-derived components in an oceanic volcano: evidence from matrix glasses and glass inclusions from Loihi seamount, Hawaii. *Chemical Geology*, *156*(1-4), 299-319.

Kurz, M. D., Jenkins, W. J., Hart, S. R., & Clague, D. (1983). Helium isotopic variations in volcanic rocks from Loihi Seamount and the Island of Hawaii. *Earth and Planetary Science Letters*, *66*, 388-406.

Kyser, T. K., & O'Neil, J. R. (1984). Hydrogen isotope systematics of submarine basalts. *Geochimica et Cosmochimica Acta*, *48*(10), 2123-2133.

Kyser, T. K., O'Neil, J. R., & Carmichael, I. S. (1982). Genetic relations among basic lavas and ultramafic nodules: evidence from oxygen isotope compositions. *Contributions to Mineralogy and Petrology*, *81*(2), 88-102.

Lassiter, J.C., Hauri, E.H. (1998). Osmium-isotope variations in Hawaiian lavas: evidence for recycled oceanic lithosphere in the Hawaiian plume. *Earth & Planetary Science Letters, 164,* 483-496.

Lassiter, J. C., Anderson, D. W., Villanueva-Lascurain, D., Marshall, E. W., & Barnes, J. D. (2022). Xenolith Constraints on "Self-Assimilation" and the Origin of Low δ 18 O Values in Mauna Kea Basalts. *Isotopic Constraints on Earth System Processes*, 133-166.

Lynn, K. J., Garcia, M. O., Shea, T., Costa, F., & Swanson, D. A. (2017). Timescales of mixing and storage for Keanakāko ʻi Tephra magmas (1500–1820 CE), Kīlauea Volcano, Hawai ʻi. *Contributions to Mineralogy and Petrology*, *172*(9), 1-20.

Lōʻihi Science Team: Duennenbier, F. K., Becker, N. C., Caplan-Auerbach, J., Clague, D. A., Cowen, J., Cremer, M., ... & Wheat, C. G. (1997). Researchers rapidly respond to submarine activity at Loihi volcano, Hawaii. *Eos*, *78*(22), 229.

Le Maitre, R.W. (Ed.), Streckeisen, A., Zanettin, B., Le Bas, M. J., Bonin, B., Bateman, P., Bellieni, G., Dudek, A., Efremova, S., Keller, J., Lamere, J., Sabine, P. A., Schmid, R., Sorensen, H., Woolley, A. R. (2002). Igneous rocks: a classification and glossary of terms, recommendations of the International Union of Geological Sciences, Subcommision of the Systematics of Igneous Rocks. Cambridge University Press, Cambridge.

Loewen, M. W., Graham, D. W., Bindeman, I. N., Lupton, J. E., & Garcia, M. O. (2019). Hydrogen isotopes in high 3He/4He submarine basalts: Primordial vs. recycled water and the veil of mantle enrichment. *Earth and planetary science letters*, *508*, 62-73.

Lynn, K. J., Garcia, M. O., Shea, T., Costa, F., & Swanson, D. A. (2017a). Timescales of mixing and storage for Keanakāko ʻi Tephra magmas (1500–1820 CE), Kīlauea Volcano, Hawai ʻi. *Contributions to Mineralogy and Petrology*, *172*(9), 1-20.

Malahoff, A., McMurtry, G. M., Wiltshire, J. C., & Yeh, H. W. (1982). Geology and chemistry of hydrothermal deposits from active submarine volcano Loihi, Hawaii. *Nature*, *298*(5871), 234-239.

Marske, J. P., Pietruszka, A. J., Weis, D., Garcia, M. O., & Rhodes, J. M. (2007). Rapid passage of a small-scale mantle heterogeneity through the melting regions of Kilauea and Mauna Loa Volcanoes. *Earth and Planetary Science Letters*, *259*(1-2), 34-50.

Martin, E., Bindeman, I., Balan, E., Palandri, J., Seligman, A., & Villemant, B. (2017). Hydrogen isotope determination by TC/EA technique in application to volcanic glass as a window into secondary hydration. *Journal of Volcanology and Geothermal Research*, *348*, 49-61.

Mattey, D., Lowry, D., & Macpherson, C. (1994). Oxygen isotope composition of mantle peridotite. *Earth and Planetary Science Letters*, *128*(3-4), 231-241.

Matzen, A. K., Baker, M. B., Beckett, J. R., & Stolper, E. M. (2011). Fe–Mg Partitioning between Olivine and High-magnesian Melts and the Nature of Hawaiian Parental Liquids. *Journal of Petrology*, *52*(7-8), 1243–1263.

Michael, P. J., & Schilling, J. G. (1989). Chlorine in mid-ocean ridge magmas: evidence for assimilation of seawater-influenced components. *Geochimica et Cosmochimica Acta*, *53*(12), 3131-3143.

Moore, J. G., Clague, D. A., & Normark, W. R. (1982). Diverse basalt types from Loihi seamount, Hawaii. *Geology*, *10*(2), 88-92.

Muehlenbachs, K., and R. N. Clayton (1976). Oxygen isotope composition of the oceanic crust and its bearing on seawater, *Journal of Geophysical Research*, *81*, 4365–4369.

Muehlenbachs, K. (1998). The oxygen isotopic composition of the oceans, sediments and the seafloor. *Chemical Geology*, *145*(3-4), 263-273.

Pietruszka, A. J., & Garcia, M. O. (1999). A rapid fluctuation in the mantle source and melting history of Kilauea Volcano inferred from the geochemistry of its historical summit lavas (1790–1982). *Journal of Petrology*, *40*(8), 1321-1342.

Pietruszka, A. J., Keyes, M. J., Duncan, J. A., Hauri, E. H., Carlson, R. W., & Garcia, M. O. (2011). Excesses of seawater-derived 234U in volcanic glasses from Loihi Seamount due to crustal contamination. *Earth and Planetary Science Letters*, *304*(1-2), 280-289.

Pietruszka, A. J., Norman, M. D., Garcia, M. O., Marske, J. P., & Burns, D. H. (2013). Chemical heterogeneity in the Hawaiian mantle plume from the alteration and dehydration of recycled oceanic crust. *Earth and Planetary Science Letters*, *361*, 298–309.

Pietruszka, A. J., Heaton, D. E., Marske, J. P., & Garcia, M. O. (2015). Two magma bodies beneath the summit of Kīlauea Volcano unveiled by isotopically distinct melt deliveries from the mantle. *Earth and Planetary Science Letters*, *413*, 90-100.

Pietruszka, A. J., Marske, J. P., Heaton, D. E., Garcia, M. O., & Rhodes, J. M. (2018). An isotopic perspective into the magmatic evolution and architecture of the rift zones of Kīlauea Volcano. *Journal of Petrology*, *59*(12), 2311-2352.

Pietruszka, A. J., Garcia, M. O., & Rhodes, J. M. (2021). Accumulated Puʻu ʻŌʻō magma fed the voluminous 2018 rift eruption of Kīlauea Volcano: evidence from lava chemistry. *Bulletin of Volcanology*, *83*(9), 1-18.

Rison, W., & Craig, H. (1983). Helium isotopes and mantle volatiles in Loihi Seamount and Hawaiian Island basalts and xenoliths. *Earth and Planetary Science Letters*, *66*, 407-426.

Roeder, P. L., & Emslie, R. (1970). Olivine-liquid equilibrium. *Contributions to mineralogy and petrology*, *29*(4), 275-289.

Shamberger, P. J., & Garcia, M. O. (2007). Geochemical modeling of magma mixing and magma reservoir volumes during early episodes of Kīlauea Volcano's Pu ʻu ʻŌ ʻō eruption. *Bulletin of Volcanology*, *69*(4), 345-352.

Shanks, W. C., Boehlke, J. K., & Seal, R. R. (1995). Stable isotopes in mid-ocean ridge hydrothermal systems: Interactions between fluids, minerals, and organisms. *Geophysical Monograph-American Geophysical Union*, *91*, 194-194.

Staudigel, H., Davies, G. R., Hart, S. R., Marchant, K. M., & Smith, B. M. (1995). Large scale isotopic Sr, Nd and O isotopic anatomy of altered oceanic crust: DSDP/ODP sites417/418. *Earth and Planetary Science Letters*, *130*(1-4), 169-185.

Swanson, D. A., Rose, T. R., Mucek, A. E., Garcia, M. O., Fiske, R. S., & Mastin, L. G. (2014). Cycles of explosive and effusive eruptions at Kīlauea Volcano, Hawai ʻi. *Geology*, *42*(7), 631-634.

The Lōʻihi Science Team (1997). Researchers rapidly respond to submarine activity at Loihi volcano, Hawaii. *Eos*, *78*(22), 229.

Wallace, P., & Carmichael, I. S. (1992). Sulfur in basaltic magmas. *Geochimica et Cosmochimica Acta*, *56*(5), 1863-1874.

Wang, Z., & Eiler, J. M. (2008). Insights into the origin of low-δ18O basaltic magmas in Hawaii revealed from in situ measurements of oxygen isotope compositions of olivines. *Earth and Planetary Science Letters*, *269*(3-4), 377-387.

Wang, Z., Kitchen, N. E., & Eiler, J. M. (2003). Oxygen isotope geochemistry of the second HSDP core. *Geochemistry, Geophysics, Geosystems*, *4*(8).

Wang, Z., Eiler, J. M., Asimow, P. D., Garcia, M. O., & Takahashi, E. (2010). Oxygen isotope constraints on the structure and evolution of the Hawaiian Plume. *American Journal of Science*, *310*(8), 683-720.

Wheat, C. G., Jannasch, H. W., Plant, J. N., Moyer, C. L., Sansone, F. J., & McMurtry, G. M. (2000). Continuous sampling of hydrothermal fluids from Loihi Seamount after the 1996 event. *Journal of Geophysical Research: Solid Earth*, *105*(B8), 19353-19367.

Wright, T. L., & Fiske, R. S. (1971). Origin of the differentiated and hybrid lavas of Kilauea volcano, Hawaii. *Journal of Petrology*, *12*(1), 1-65.

Yang, H. J., Frey, F. A., Rhodes, J. M., Garcia, M. O. (1996). Evolution of Mauna Kea volcano: Inferences from lava compositions recovered in the Hawai'i Scientific Drilling Project. *Journal of Geophysical Research, 101*(B5), 11747-11767.